Morphogenetic ovarian modules for oocyte production from germline stem cells

Yaniv Elkouby

yaniv.elkouby@mail.huji.ac.il

The Hebrew University of Jerusalem, School of Medicine https://orcid.org/0000-0002-9043-4106

Neta Hart

The Hebrew University of Jerusalem, School of Medicine

Johanna Kroll

Max Delbrück Center for Molecular Medicine in the Helmholtz Association https://orcid.org/0000-0003-4652-3598

Vineet Kumar

The Hebrew University of Jerusalem, Faculty of Medicine

Sylwia Czukiewska

Leiden University Medical Center https://orcid.org/0000-0001-9151-9008

Yoel Bogoch

The Hebrew University of Jerusalem, School of Medicine

Noga Guler

The Hebrew University of Jerusalem, School of Medicine https://orcid.org/0009-0004-8560-1995

Karine Levy

The Hebrew University of Jerusalem, Faculty of Medicine https://orcid.org/0000-0003-0290-062X

Susana Chuva de Sousa Lopes

Leiden University Medical Center

Jan Philipp Junker

Max Delbrück Center for Molecular Medicine https://orcid.org/0000-0002-2826-8290

Biological Sciences - Article

Keywords:

Posted Date: October 28th, 2025

DOI: https://doi.org/10.21203/rs.3.rs-7325126/v1

Additional Declarations: There is **NO** Competing Interest.

Morphogenetic ovarian modules for oocyte production from germline stem cells

Neta Hart[1,2#], Johanna B. Kroll[3,4#], Vineet Kumar[1,2], Sylwia M. Czukiewska[5,6], Yoel Bogoch[1,2], Noga Guler[1,2], Karine Levy[1,2], Susana M Chuva de Sousa Lopes[5,6], Jan Philipp Junker[3,4,7], and Yaniv M. Elkouby[1,2*]

[1] Department of Developmental Biology and Cancer Research, The Hebrew University of Jerusalem Faculty of Medicine, Ein-Kerem Campus, Jerusalem, Israel 9112102

[2] Institute for Medical Research – Israel-Canada (IMRIC), Ein-Kerem Campus, Jerusalem, Israel 9112102

[3] Laboratory for Quantitative Developmental Biology, Berlin Institute for Medical Systems Biology, Max Delbrück Center for Molecular Medicine in the Helmholtz Association, Berlin, Germany

[4] Charité – Universitätsmedizin Berlin, Germany

[5] Department of Anatomy and Embryology, Leiden University Medical Center, 2333 ZC Leiden, the Netherlands

[6] The Novo Nordisk Foundation Center for Stem Cell Medicine (reNEW), Leiden University Medical Center, 2333 ZC Leiden, The Netherlands

[7] German Center for Cardiovascular Research (DZHK), Site Berlin, Berlin, Germany

[#]These authors contributed equally

*Corresponding author. Email: yaniv.elkouby@mail.huji.ac.il

Abstract

Oocyte production from early progenitors in the fetal ovary determines the ovarian reserve and impacts lifelong female reproduction, yet its developmental regulation remains elusive. Early progenitors or germline stem cells (GSCs) are not maintained in adult mammalian ovaries, and in mice they are lost closely following embryonic sex determination. Fundamental knowledge of vertebrate ovarian GSCs and how they are regulated to produce oocytes in the developmental context of the ovary is lacking. Here, we uncover a previously unrecognized ovarian developmental microenvironment, the ovarian module, in developing zebrafish and human ovaries. We show zebrafish ovarian modules comprise the morphogenetic unit of oocyte production, harboring GSCs at the young tip, which generate oocyte precursors and early differentiating oocytes in a spatially linear manner. We define module morphology, resolve its developmental dynamics, recapitulate its single-cell transcriptomic architecture, and identify Notch signaling as a regulator of GSCs. We map Notch pathway components in modules, identifying GSC as sender cells and their progeny as receiver cells, and functionally demonstrate that Notch activity is required to suppress the GSC fate and to promote differentiation. Ovarian modules persist in adult zebrafish ovaries, highlighting a similar framework in oocyte production during homeostasis. We further demonstrate that modules are conserved in human fetal ovaries, where POU5F1/OCT4+ germ cells and differentiating oocytes are similarly organized, and Notch components are expressed in equivalent cell types, supporting the module as a fundamental strategy in oocyte production. Our findings propose new developmental principles for oogenesis and establish new paradigms in female GSC biology and for women's reproductive regenerative medicine.

Introduction

Stem cells are essential to construct lineages of differentiating cells, build organs in development, and repair them during homeostasis. Germline stem cells (GSC) produce differentiating oocytes through the process of oogenesis, which is requisite for fertility, embryonic development, and reproduction. Extensive studies in the Drosophila gonads and in the mouse testis have characterized somatic niches, and identified niche-GSC interactions and other factors that control GSC self-renewal and differentiation, yielding established paradigms in GSC biology (reviewed in[1,2,3,4]). In contrast, fundamental knowledge of ovarian GSCs in vertebrates is lacking.

In the developing mammalian ovary, early oocyte precursors are short lived and their regulation is coupled with sex determination (rev. in[5]). In the male, fetal spermatogonial precursors enter a G0 state and are maintained as GSCs throughout life[5]. In the female mouse, meiosis induction synchronously initiates differentiation of germ cells in the fetal ovary closely following sex determination[5]. The essential male determinant FGF9[6] promotes maintenance of pluripotency markers and inhibits meiosis[7,8,9]. In *fgf9*$^{-/-}$ XY gonads, pluripotency markers are lost, meiosis is precociously induced and germ cells differentiate as oocytes, resulting in male to female sex-reversal[7,8,9]. This suggests that in the mouse, maintenance of early germ cells as GSCs and female differentiation are mutually exclusive. Consistently, the convention is that in post-natal mammalian ovaries, GSCs are not maintained[5]. Recent reports that suggest the existence of GSC-like or mitotic germ cells in adult ovaries[10,11] remain controversial[12]. This creates an experimental barrier to investigating the regulatory mechanisms that control GSCs and their production of oocytes in mammals.

Unlike in the mouse, in the human fetal ovary meiosis induction and subsequent early oocyte differentiation is not synchronous[13,14,15]. Oocyte progenitors reside adjacent to oocytes during at least 20 weeks of post-gestation development[13,14,15]. However, how oocyte progenitors are maintained and produce oocytes during this developmental time-frame is poorly understood in humans. In humans, early oogenesis from the early mitotic progenitors to the primary follicle is executed in the developing fetal ovary, and the lack of GSC maintenance postnatally precludes later oocyte production. Thus, early oogenesis in the fetus determines by birth the number and quality of eggs for the entire person‘s lifespan. Defects in early oocyte and ovarian development are a leading cause for miscarriages and infertility, as well as reproductive syndromes and

malignancies, but the mechanistic defects are unknown because we lack a fundamental understanding of these early processes.

An excellent model for understanding the biology of human GSCs is presented by the zebrafish ovary. In contrast to the mouse and similar to the human fetal ovary, in the zebrafish ovary, GSCs and mitotic oocyte precursors neighbor differentiating meiotic oocytes. As major oogenesis processes are conserved, the zebrafish is an excellent model for human oogenesis[16]. One prominent characteristic is advantageously unique to zebrafish: unlike in mammals, zebrafish GSCs are maintained and actively produce oocytes throughout life[17,18], and zebrafish ovaries have tremendous regenerative capacity, driven by GSCs that replenish the oocyte pool upon injury or genetic ablation[18]. Thus, zebrafish ovarian GSCs provide an excellent opportunity to investigate female GSCs in a vertebrate context in both development and regeneration.

A conserved regulator of GSC maintenance is Nanos2 (Nos2), an mRNA binding protein that post-translationally represses expression of meiotic genes[19,20,21,22]. In humans, mutations in *NANOS2* were identified in sterile men[23] indicating its conserved importance. In fish, *Nos2* is a marker of both male and female GSCs[17,24], and key similarities exist between fish and mammal GSCs: ***1)*** Fish and mouse GSCs specifically express *nos2*. ***2)*** In *nos2*$^{-/-}$ and *nos3*$^{-/-}$ zebrafish gonads, GSCs are initially specified but not maintained, and differentiating meiotic oocytes are lost[17,18]. This is consistent with mammals, where Nos2 is required for GSC maintenance and acts partially redundantly with Nos3[17,18,25]. ***3)*** Two cell populations were identified in the mouse testis: long lived *nos2*+ GSC and short lived *ngn3*+ transit amplifying cell[26,27]. Consistently with this, two similar GSC populations, *nos2*+ slow cycling and *nos2(-)* fast cycling GSCs were identified in the teleost fish Medaka[24].

However, despite these advances, fundamental questions remain open for both zebrafish and human. How GSCs are maintained and protected from differentiation signals that act upon neighboring meiotic oocytes is unknown. Potential interactions with a somatic niche, are unclear. A niche for *nos2*+ GSCs at the surface of the ovary was indicated in Medaka but was not investigated functionally[24]. In zebrafish, *nos2*+ GSCs were suggested to reside at the surface of the ovary[17], but a niche was not identified. Further, the molecular identity of GSCs, their spatial organization in the ovary, and the morphological processes by which they divide, self-renew, and differentiate are poorly understood. Finally, it is unclear how GSCs, progenitors, mitotic and

differentiating cells, as well as supporting somatic cells and potential niches, are developmentally organized to produce oocytes.

Results

Newly identified ovarian modules as morphogenetic units of oocyte production

To study the early production of oocytes from GSCs, we investigated the developing ovary of juvenile fish at post-embryonic stages, which provides an ideal system[28] to resolve elusive developmental dynamics of early oogenesis[29,30,31,32,33,34], including those from GSCs to early differentiating oocytes. GSCs give rise to mitotically dividing oocyte precursors, called oogonia (Fig. 1a). Oogonia undergo several rounds of divisions with incomplete cytokinesis, resulting in persistent cytoplasmic bridges (CBs) between daughter cells[30,35,36,37,38]. These incomplete divisions generate a conserved cellular organization, called the germline cyst - a cluster of interconnected germ cells surrounded by somatic pre-granulosa cells[30,31,35,36,37,38,39] (Fig. 1a). Oocyte differentiation, initiated with the induction of meiosis, begins within the germline cyst (Fig. 1a). In both zebrafish and mice, oocytes continue to develop in the cyst and only leave it to form the primordial follicle by pachytene stages[16,31] (Fig. 1a). The cyst serves as a hub for major essential processes in early oogenesis[31], yet the mechanisms underlying its formation in vertebrates are still unclear[31].

We analyzed the organization of the cyst hub in developing zebrafish ovaries and identified a higher-order arrangement of cysts. In ovaries, we found cysts spatially arrayed from mitotic oogonia at the young tip, through progressive stages of meiotic differentiation (leptotene and zygotene stages of meiotic prophase), to oocytes initiating follicle formation at the zygotene–pachytene transition[37], positioned at the old tip (Fig. 1a-c). Oocytes were staged as previously determined[28,30]. Multiple such arrangements were scattered throughout the ovaries. We termed these higher-order arrangements ovarian modules and hypothesized that they could reflect morphological patterns of oocyte production and indicate the spatial localization of GSCs.

We characterized the morphology of ovarian modules. The germline cyst is considered the developmental unit of oocytes. Based on data from mice, all germ cells within a cyst are at the same developmental stage and progress synchronously[31,40,41,42]. Each cyst is also individually encapsulated by somatic cells[31,40,41,42]. Strikingly, our observations suggest that groups of oocytes at individual stages—previously thought to belong to separate cysts—are likely

organized at a higher level within the module. We focused on two key features of cysts: ***1)*** their physical separation by somatic cell encapsulation, and ***2)*** the developmental synchrony of interconnected germ cells within cysts, which arises from incomplete mitotic divisions of oogonia.

First, three-dimensional confocal microscopy of wholemount ovaries, revealed that cells in modules appeared intimately interfacing one another as shown by labeling of their cell cortex, indicating that they may not be separated by somatic cells (Fig. 1d). Labeling with a somatic marker, showed that somatic cells wrapping around the module do not invade or separate groups of oocytes at distinct stages within the module. To label somatic cells we used the transgenic line *Tg(ub:zebrabow)*[43], which specifically drives mRFP expression in somatic cells but not germ cells in ovaries[29]. Transgenically-labeled somatic cells clearly engulfed module cells (Fig. 1e), containing oocyte groups at consecutive stages, as defined by morphological criteria[28,30] (Fig. 1e-f). However, these labeled somatic cells did not invade, or only partially invaded, the vicinity of the module, leaving open spaces or gaps between oocyte groups at different stages (Fig. 1e, g and Supplementary Video 1). This was confirmed by expression of the oogonia stage-specific marker gene *foxl2l*[44,45] as detected by HCR-FISH, where *foxl2l* (+) and *foxl2l* (-) cells residing the same module, were not separated by transgenically-labeled somatic cells (Fig. 1h-j, Supplementary Video 2). To further confirm this observation, we analyzed ovaries using serial block-face scanning electron microscopy (SBF-SEM), which generates three-dimensional views of entire cysts at EM resolution, as previously shown[30]. This analysis unequivocally demonstrated that while module cells are separated from outer tissue by somatic cell membranes (Fig. 1k, Supplementary Video 3), leptotene and zygotene cells within modules maintain continuous cell–cell interfaces along the entire z-axis, with no additional cytoplasmic membranes from other cells between them (Fig. 1k, Supplementary Video 3). These data demonstrate that multiple cysts are collectively engulfed by somatic cells within modules.

Second, we analyzed the developmental synchrony of inter-connected germ cells in cysts, by labeling for the midbody marker Cep55l in CBs between sister cells[30,46]. Cep55l-positive midbodies were detected between germ cells at different developmental stages (Fig. 1l and Supplementary Videos 4-5), suggesting connectivity through CBs generated during earlier mitotic divisions of oogonia. Specifically, Cep55l-labeled midbodies were clearly visible between *foxl2*+ oogonia and *rec8*+ oocytes at meiotic entry (Fig. 1l and Supplementary Videos 4), and

similarly between *rec8*+ oocytes at meiotic entry and *dmc1*+ oocytes in progressive meiotic prophase (Fig. 1l and Supplementary Videos 5). The interconnectivity between germ cells at distinct developmental stages demonstrates that cysts are developmentally non-synchronous and strongly suggests that groups previously thought to represent independent developing cysts are organized into a higher-order structure. These data support the idea that the module functions as a previously unrecognized morphogenetic unit of oocyte development and potentially reveals a novel mode of oocyte production.

Ovarian modules comprise the developmental microenvironment of oocyte production from GSCs

The newly identified developmental unit of the module suggests spatially regulated oocyte production from GSCs and predicts GSC localization at the young tip of the module, adjacent to oogonia. To test this, we labeled GSCs by HCR-FISH for *nos2*. Strikingly, *nos2*+ GSCs were detected at the young tip of modules, adjacent to oogonia (Fig. 2a-c), consistent with the prediction. Co-labeling of *nos2* by FISH with immunostaining for the germ cell-specific marker Ddx4 confirmed the identity of *nos2*+ cells as germ cells (Extended Data Fig. 1a). Size measurements of *nos2*+ GSCs, performed using criteria established for oocyte size quantification[28,30], showed that *nos2*+ GSCs (10.3 ± 1.23 μm in diameter; Extended Data Fig. 1b) fall within the same size range as oogonia[28,30,37]. These findings indicate that a subset of cells previously identified as oogonia are GSCs, as previously proposed[17], and further support GSC localization adjacent to oogonia at the young tip of modules.

We characterized the distribution of *nos2*+ GSCs in ovaries. While a minority of *nos2*+ GSCs were located apart from oogonia, the majority were positioned immediately adjacent to oogonia (Fig. 2a-c and Extended Data Fig. 1c). In most instances where *nos2*+ GSCs resided next to oogonia, additional progressive oocyte stages were also present (Fig. 2a-c and Extended Data Fig. 1c), suggesting that these configurations likely represent snapshots of module formation. Most *nos2*+ GSCs appeared in clusters of 2–4 cells, with some groups containing up to 7 cells (Extended Data Fig. 1d), although a few were solitary. Consistent with this, co-labeling of *nos2* by FISH with immunostaining for the mitotic marker pHH3 showed that some *nos2*+ GSCs were actively dividing, while others were not (Extended Data Fig. 1e). The variability in GSC group size, localization at the young tip of developing modules, and heterogeneous mitotic states suggests the existence of potential subpopulations of *nos2*+ GSCs, possibly

corresponding to different phases of module construction. These findings provide evidence for the spatial organization of ovarian GSCs and their role in oocyte production.

To confirm the spatial linear development of oocytes from GSCs within modules, we analyzed expression patterns of stage-specific oocyte developmental marker genes by HCR-FISH in whole ovaries. We examined the expression of *nos2* (GSCs[17,18]) *foxl2l* (oogonia[44,45]), *rec8* (meiotic entry[45]), and *dmc1* (progressive meiotic prophase[45,49,50]). Modules exhibited a clear developmental sequence: *nos2*+ cells at the young tip, followed by a cluster of *foxl2*+ cells, then a cluster of *rec8*+ cells, and finally a cluster of *dmc1*+ cells (Fig. 2d-g), which was confirmed by the normalized intensity of each marker along modules (Fig. 2d-g). For each developmental stage, only a minority of expression clusters were detected independently of modules, while the vast majority were found within modules (Fig. 2k). Multiplexed HCR-FISH for combinations of these marker genes and their measured normalized intensities along modules (Fig. 2h-j), validated the linear organization of consecutive developmental stages within modules. For each marker, positively expressing clusters were adjacent to clusters expressing the preceding stage's marker in the vast majority of cases (Fig. 2l), further supporting a linear developmental progression.

Furthermore, we detected instances within modules where expression of distinct marker genes from developmentally consecutive clusters overlapped in cells located at the interface between the two clusters. E.g., we detected cells co-expressing *nos2* and *foxl2l* at the margins between *nos2*+ cluster and *foxl2l*+ cluster (Extended Data Fig. 1f), cells co-expressing *foxl2l* and *rec8* and the margin of their clusters (Extended Data Fig. 1g), and cells co-expressing *rec8* and *dmc1* at the margin of their clusters (Extended Data Fig. 1h). Co-expression of those markers was confirmed by overlapping normalized intensities of each marker at the appropriate positions along modules (Extended Data Fig. 1f-h). The distribution of all oocytes expressing a single- or two consecutive developmental marker genes is plotted in Extended Data Fig. 1i. A simple interpretation of these cases is that cells with overlapping expression are likely transitioning between developmental stages, progressively shifting expression from one developmental marker to the next. These spatially linear and progressive gene expression patterns strongly support the spatially ordered development of oocytes within modules.

We confirmed these findings in an unbiased manner using our automated segmentation tools, developed for the analysis of germline cysts[31]. We optimized these tools to segment stage-

specific clusters based on HCR-FISH signals in three-dimensional (3D) images of whole ovaries (Methods and Extended Data Fig. 2). For each stage-specific cluster, we tested whether another cluster was located nearby in 3D. Clusters within half a cell diameter (based on an average size of the sizes of each of the oogonia, leptotene, and zygotene stages) were considered likely to be interfacing and were scored as adjacent, while clusters beyond this range were not (Methods and Extended Data Fig. 2). We next analyzed the distribution of developmental stages in adjacent clusters relative to each reference cluster in pairwise comparisons (Methods and Extended Data Fig. 2). This analysis revealed that, as demonstrated above, the majority of clusters were adjacent to a cluster of cells at the immediately preceding stage (Fig. 2m-n). As further evidence, the analysis also showed that *nos2*+ and *rec8*+ clusters, which represent non-consecutive stages, were only rarely found adjacent to one another (Fig. 2o), likely reflecting chance proximity of distinct modules. These results provide further unbiased support for a linear developmental progression of oocytes from GSCs through modules.

Dynamics of module development

To determine whether oocytes develop linearly within modules, we lineage-traced module cells from early progenitors. We used a floxed-STOP cassette driving *mCherry* expression upon recombination by a heat-shock-inducible *Cre-ERT2*[51,52,53]. To visualize clones, we induced partial recombination, detected by nuclear mCherry signals, in a subset of *Ddx4*+ primordial germ cells (PGCs) at larval stages (Methods and Extended Data Fig. 3a). We then traced mCherry+ lineages in early developing ovaries at 4–5 weeks post-fertilization (wpf), where partial labeling of developing germ cells was confirmed (Methods and Extended Data Fig. 3b).

Analysis of *mCherry*+ lineages in ovaries co-labeled with multiplexed HCR-FISH for *nos2* and *foxl2l,* and for *foxl2l* and *rec8* revealed clonal trajectories within modules. Specifically, we detected three types of traced clusters. Two of these types were (Fig. 3a-b): ***1)*** fully *mCherry*-labeled stage-specific clusters, in which all cells within a cluster were *mCherry*+ (Fig. 3a-b top), and ***2)*** fully *mCherry*-unlabeled stage-specific clusters, in which all cells per cluster were *mCherry (-)* (Fig. 3a-b bottom). The distribution of all categories of traced clusters is plotted in Fig. 3d-e. In these cases, fully labeled clusters at a given stage were adjacent to fully labeled clusters of the preceding stage. Specifically, *mCherry*+ *nos2* and *foxl2l* clusters were adjacent (Fig. 3a top, f), as were *mCherry*+ *foxl2l* and *rec8* clusters (Fig. 3b top, g). These clonal trajectories suggest that germ cells at successive developmental stages are derived from their immediate precursors

within modules. Together with our previous findings, these data indicate that GSCs at the young tip of modules give rise to lineages of developing oogonia and oocytes in a spatially organized manner.

Interestingly, we identified a third type of traced *nos2*+, *foxl2l*+, and *rec8*+ clusters, in which both *mCherry*+ and *mCherry (-)* cells were found; we termed these partially labeled clusters (Fig. 3c). This partially labeled cluster category, along with the fully-labeled and fully unlabeled categories, was confirmed by co-staining for mCherry and Ddx4 (Extended Data Fig. 3c), but represented a minority of the three categories (Fig. 3d-e). This finding indicates the presence of two or more clones in modules. We analyzed the distribution of partially labeled clusters within modules and found that either fully or partially labeled clusters were adjacent to either fully or partially labeled clusters at the preceding stage: fully/partially labeled *foxl2l*+ clusters were adjacent to fully/partially labeled *nos2*+ clusters (Fig. 3f), and fully/partially labeled *rec8*+ clusters were adjacent to fully/partially labeled *foxl2l*+ clusters (Fig. 3g). These findings support linear development within modules and further suggest the presence of two or more clones within a single module.

Notably, partially labeled clusters could potentially result from cyst fragmentation and coalescence into non-clonal clusters, which was shown in mice[41] upon PGC entry into the gonad[54]. However, in zebrafish PGCs entry into the gonad occurs much earlier during embryonic development and is unlikely directly relevant to developmental progression within modules. In any case, partially labeled clusters represented only a minority of traced clusters (Fig. 3d-e). Thus, while we cannot formally rule out the existence of such behaviors, they are unlikely to make a major direct contribution to developmental progression within organized modules in zebrafish.

To gain further insight into the dynamics of module construction, we analyzed mitotic divisions of oogonia. Labeling ovaries with the mitotic marker phospho-Histon H3 (pHH3) showed that oogonia divide in a non-synchronous manner. While some cysts displayed homogeneous pHH3 signals across the nuclei of all cells, indicating synchronous divisions, most cysts exhibited a heterogeneous mix of pHH3-positive and -negative nuclei, demonstrating non-synchronous divisions (Fig. 3h-i, k). Live time-lapse imaging of oogonial divisions in whole ovaries transgenically expressing *H2A-GFP* confirmed these findings. While some cases showed synchronous divisions in real time, most clearly exhibited non-synchronous divisions (Fig. 3j, l,

Extended Data Fig. 3d and Supplementary Video 6-9). Furthermore, while we detected CBs between *foxl2l*+ and *rec8*+ cells, and between *rec8*+ and *dmc1*+ cells (Fig. 1l), we never detected CBs between *nos2*+ and *foxl2l*+ cells (Extended Data Fig. 1j). The absence of stabilized CBs between *nos2*+ and *foxl2l*+ cells suggests that interconnected cysts form at the level of *foxl2l*+ oogonia, not at the level of *nos2*+ GSCs. Together with our lineage tracing results, these data suggest that more than one clone of GSCs at the young tip of modules, produce oogonia that divide asynchronously and then progress through meiosis along modules (see Discussion).

Profiling ovarian cell types identifies the Notch signaling pathway as a regulator of GSCs and oocyte differentiation in modules

Next, we sought to complement our spatial characterization of the ovarian modules with a detailed temporal analysis of the oocyte differentiation trajectory. We reasoned that single-cell RNA-sequencing (scRNA-seq) followed by pseudotemporal trajectory reconstruction[55] of 5 wpf ovaries would allow us to identify novel regulators of GSC identity and oocyte differentiation. As pointed out by recent studies, scRNA-seq analysis of the ovary is challenging due to cell type selection biases and background contamination (ambient RNA) upon dissociation[45,56,57]. We therefore set out to optimize the experimental and computational pipeline to address these tissue specific challenges (Fig. 4a). In particular, we found that using a pool-and-split approach and working with fixed cells led to better results (Methods). Furthermore, we performed separate quality filtering for oocytes compared to other cell types, since oocytes have much higher RNA content due to their larger size (Methods and Extended Data Fig. 4). In summary, we obtained a dataset consisting of 9331 cells with 3159 germ cells (Extended Data Table 1).

In this new dataset we detected the expected major cell types: follicle cells, pre-follicle cells, vasculature and immune cells, as well as 5 clusters of other somatic gonadal cells (Fig. 4b), which we annotated based on established marker genes[45,58,59,60,61,62] (Fig. 4c and Extended Data Table. 2). While we did not identify a clear theca cell population (cyp11a2 pos.), we observed that somatic cluster 3 shows some cyp11a2 expression and might hence correspond to theca cells.

To gain insight into differentiation dynamics in oogenesis, we next performed a sub-clustering of the oocyte cells. This analysis recapitulated the known progression of the marker genes *nos2* (GSCs), *foxl2l* (oogonia), *rec8a* (meiotic entry) and *dmc1* (prophase oocytes) in the first four clusters (Fig. 4d and Extended Data Table 3), highlighting that the transcriptomic

analysis recapitulates the module architecture by correlating strongly with the findings on cell type progression in microscopy experiments. We validated these results with a second dataset generated with conventional droplet microfluidics, albeit with lower data quality due to ambient RNA (Extended Data Fig. 5).

Next, we sought to identify pathways with a potential regulatory role in early oogenesis and formation and/or maintenance of module architecture. To this end, we modelled a pseudotime trajectory over the oocyte sub-clustering, which enabled us to visualize marker gene expression along the module (Fig. 4e, Methods). We reasoned that putative regulators of cell state transitions would follow similar expression trajectories as these marker genes. We therefore searched for genes whose expression dynamics were correlated to the marker genes of the first four clusters (*nos2, foxl2l, rec8a* and *dmc1*) (Fig. 4f-g). The top genes correlating to *nos2* (i.e. putative regulators for the transition from GSCs to oogonia) included known stem cell regulators, such as the histone methyltransferase *kmt2bb* (within the top ten, Fig. 4g) and the DNA methyltransferase *dnmt3bb.1* (ranked 11th, Extended Data Table 4). Both Kmt2b and Dnmt3b perform key epigenic regulation of stem cells in human and mice, essential for stem cell-to-progenitor transition[63,64,65], with Kmt2b being highly expressed in mouse spermatogonial stem cells where it exerts this function[63]. The detection of these genes underscores the efficiency of our strategy and highlights major epigenetic regulation in early oogenesis[56].

Interestingly, *jag2b*, a ligand in the Notch signaling pathway, stood out as an enriched element of a cell-cell signaling pathway (Fig. 4g). Furthermore, *notch2* was also correlated with the marker for meiotic entry *rec8a* (Extended Data Fig. 6 and Extended Data Table 4). Indeed, when scoring expression of genes related to Notch signaling, we observed a distinct pattern of Notch activation in the early stages of the inferred differentiation trajectory (Fig. 4h). In summary, we recapitulated the module architecture transcriptomically, which allowed us to identify Notch signaling as a potential regulator of the early stages of GSC differentiation.

Notch signaling suppresses the GSC fate and promotes oocyte differentiation in modules

To address the involvement of Notch signaling in controlling GSCs and oocyte production within modules, we first mapped the expression of Notch signaling pathway components identified from our single-cell transcriptomic analyses above, in ovaries, with a focus on module cells. We validated the expression of those Notch pathway genes using HCR-FISH in whole ovaries and determined the specific cell types in which they are expressed.

We first confirmed the expression of the Notch ligand gene *jag2b* specifically in *nos2*+ GSCs. *jag2b* expression was detected in *nos2*+ cells (Fig. 5a, b left). Moreover, *jag2b* expression was excluded from *foxl2l*+ cells and was detected only in adjacent cells, which likely represent *nos2*+ GSCs (Fig. 5a, b right). Next, we examined the expression of the *notch2* and *notch3* receptors. *notch2* was expressed specifically in *foxl2l*+ cells and in some unidentified somatic cells (Fig. 5c-d). *notch3* was similarly expressed in *foxl2l*+ cells (Fig. 5e, f red box), but showed a more dynamic pattern, with some *foxl2l*+ cells lacking *notch3* expression (Fig. 5e, f green box) and *notch3* also expressed in some *foxl2l (-)* cells (Fig. 5e, f cyan box). We further found that the Notch target gene *her6* is specifically expressed in *foxl2l*+ cells and not in *nos2*+ cells (Fig. 5g-h). Altogether, this expression pattern reveals the potential directionality of Notch signaling, with *nos2*+ GSCs acting as sender cells (expressing the Jag2b ligand) and *foxl2l*+ progeny as receiver cells (expressing the Notch2 and Notch3 receptors, and the target gene *her6*). Thus, Notch pathway components are correctly positioned in both time and space within modules to regulate GSCs and their progeny.

To test the function of Notch signaling in ovaries, we utilized a recently established *ex-vivo* ovary culture system (Fig. 5i), which reliably recapitulates early oogenesis, including the development of GSC progeny, the oogonia, to primordial follicle formation[34]. This system has already been instrumental in identifying novel regulators and mechanisms, which were subsequently validated genetically *in-vivo*[34]. Specifically, at the stages relevant to the module, we observed normal divisions of somatic and germ cells, including oogonia and presumably GSCs and/or their progeny, as well as normal progression rates between oocyte developmental stages *ex-vivo*, comparable to those observed *in-vivo*[34]. Therefore, all major events of early oogenesis proceed in this system similarly to their execution under physiological conditions *in-vivo*. Indeed, in control cultured ovaries, *nos2*+, *foxl2l*+, and *rec8*+ cells were all present in normal numbers after 3 days in culture (days post-culture, dpc) (Fig. 5j-k). Moreover, we detected their developmental organization in modules, identical to that observed *in-vivo* (Fig. 5j).

To test the roles of Notch signaling, we inhibited its activity using the well-established γ-secretase inhibitor DAPT[66,67] in ovaries *ex-vivo* (Fig. 5i). γ-secretase is required for cleavage of the Notch receptor; thus, its inhibition blocks Notch signal transduction to the nucleus and prevents regulation of downstream target gene expression[66,67,68]. DAPT treatment led to a sharp increase in the number of *nos2*+ cells and a concomitant decrease in *foxl2l*+ and *rec8*+ cells (Fig.

5j-k). In addition, organized modules were no longer detected following Notch inhibition. These results demonstrate that Notch signaling is required to suppress the GSC fate and promote oocyte differentiation, providing mechanistic insight into the developmental regulation of vertebrate female GSCs and their production of oocytes via the Notch signaling pathway in modules.

Ovarian modules are preserved in adult ovarian homeostasis

Having established the ovarian modules as the developmental microenvironment for oocyte production from GSCs during development, we sought to examine their conservation during adult homeostasis. Zebrafish GSCs are maintained and actively produce oocytes throughout life[17,18]. Moreover, the regenerative capacity of zebrafish ovaries depends on GSCs, which replenish the oocyte pool following injury or genetic ablation[18]. Thus, GSC maintenance is essential not only during gonad and sexual development, but also for sustaining oocyte production and fertility during adult ovarian homeostasis. However, how GSCs are maintained and produce oocytes throughout life - and how they are spatially organized in adult ovaries - remain unknown.

We identified ovarian modules in adult ovaries that appeared identical to those observed in developing ovaries (Fig. 6a). Adult modules were embedded within the tissue and scattered among developing oocytes at later stages of oogenesis. Each module contained spatially linear germ cell clusters, with *nos2*+ GSCs at the young tip, followed by *foxl2*+ oogonia and *rec8*+ oocytes at meiotic entry (Fig. 6a), and overall appeared morphologically similar to modules in developing ovaries. Analyzing the spatial distribution of these cells as we did in developing ovaries, confirmed that clusters at specific developmental stages are found adjacent to clusters at preceding stages (Fig. 6b). Similarly to modules during development, the majority of *foxl2l*+ clusters were adjacent to *nos2*+ clusters, the majority of *rec8*+ clusters were adjacent *foxl2l*+ clusters, and *rec8*+ clusters were only rarely found adjacent to non-consecutive *nos2*+ clusters (Fig. 6b). These results strongly suggest that, as in ovarian development, oocytes are produced from GSCs through ovarian modules during adult homeostasis. A morphogenetic unit such as the module may provide an efficient morphological and mechanistic framework necessary for GSC maintenance and oocyte production, supporting both reproduction and regeneration.

Human fetal ovaries exhibit module-like organized oocyte development

As in zebrafish, a similar developmental principle of spatial-linear oocyte production from GSCs is well established in invertebrates, such as *D. melanogaster* and *C. elegans*[5,69,79]. We explored whether development in modules represent a conserved strategy of oogenesis in humans. In the second trimester of pregnancy, human fetal ovaries contain a heterogenic mix of oocytes at different developmental stages, from presumptive mitotic stages to meiotic arrest in dictyate stage[71], strongly suggesting non-synchronous development similar to zebrafish. Interestingly, we previously showed that early mitotic and meiotic stages are organized together in ovarian cords[72], implying potential developmental order, but this has not been addressed. We therefore analyzed human fetal ovaries at 19 weeks of gestation (WG), asking whether these early stages are organized developmentally in potential modules in the ovarian cords. The production of differentiating oocytes from mitotic progenitors in humans is limited to fetal development, and is critical for the reproductive health throughout the entire individual lifespan, but its underlying dynamics and mechanisms remain elusive. We reasoned that addressing their potential developmental organization will provide a timely critical insight.

To address potential developmental order in human fetal ovaries, we first analyzed the distribution of cells at progressing developmental stages, as detected by nuclear POU5F1 (also known as OCT4) (early germ cells), cytoplasmic DDX4 (oogonia and oocytes) and nuclear SYCP3 that marks meiotic onset and then progressively propagate along chromosomal axes during prophase, completing axial formation by zygotene-pachytene stages[71] (Fig. 6c). To surveil meiosis progression, we took advantage of telomere dynamics in early prophase, which is a characteristic feature of meiotic chromosomal pairing. At meiotic onset (leptotene stages) telomeres, as labeled with telomeric protein TRF1/2, are loaded on the nuclear envelope (NE), and are later clustered at one pole of the NE (zygotene stages)[50,73]. Strikingly, we found that these stages are spatially organized in a linear module-like fashion (Fig. 6c), whereby POU5F1+ cells are found at the young tip, followed by DDX4+ cells at meiotic onset-leptotene stages (telomeres are loaded radially on the NE, SYCP3 propagate along chromosomal axes), which in turn are followed by cells at zygotene stages (clustered polarized telomeres, more predominant SYCP3 staining).

We validated these cytological results by monitoring the expression of stage-specific marker genes, using HCR-FISH in human fetal ovaries. We focused on expression of *STRA8* which is induced by retinoic acid (RA) signaling and marks meiotic onset, and of meiotic-marker

SYCP3. Consistent with our results above, *SYCP3*+ cells were found in clusters adjacent to *STRA8*+ cell clusters in a module-like organization (Fig. 6d). Analyzing the spatial distribution of these cells as we did in zebrafish ovaries, we confirmed that the majority of *SYCP3*+ clusters were adjacent to *STRA8*+ clusters (Fig. 6e). Altogether, our results demonstrate that early germ cells and progressing meiotic oocytes are organized in ovarian modules in ovarian cords. These findings suggest that human ovarian modules provide the developmental microenvironment for germ cell progression from POU5F1+ cells to diplotene oocytes, similar to zebrafish.

Next, we investigated whether NOTCH signaling plays a role in the production of ovarian modules in humans, similar to its role in zebrafish. Extracting single-cell RNA-seq of human fetal ovary at 16-18WG from a curated dataset[71,74], we first confirmed cell cluster identity and developmental age (Fig. 6f, g). Our analysis revealed that the NOTCH ligands *DLL3* and *JAG2* are the primary ligands expressed in *POU5F1*+ early germ cells, while *DLK1* is expressed in *REC8*+ RA-responsive germ cells and *JAG1* is specifically expressed in diplotene germ cells. Notably, *NOTCH2* is not expressed in *POU5F1*+ early germ cells, but its expression increases in *REC8*+ RA-responsive and *SPO11*+ meiotic germ cells (Fig. 6g) and response genes *HEY1* and *HES1* upregulate towards pachytene, as in zebrafish. This suggested that human early germ cells may communicate to meiotic germ cells through NOTCH receptor–ligand interactions. Using immunofluorescence, we validated NOTCH2 expression in human DDX4+ germ cells, in particular those immediately adjacent to POU5F1+ cells, and in early meiotic germ cells with NE-loaded TRF1/2 (Fig. 6h). Together these findings are consistent with observations in zebrafish and highlight a conserved role for the NOTCH signaling pathway in linear modules in ovarian cords.

Discussion

Early oogenesis is an essential and highly dynamic process that must be precisely executed for successful reproduction, yet it remains remarkably incompletely understood. In humans, the production of primary follicles from early mitotic progenitors occurs in the developing fetal ovary and, by birth, determines the number and quality of eggs for the individual's entire lifespan - impacting the lifelong reproductive health of women. The absence of GSC maintenance postnatally precludes further de-novo oocyte production. However, the developmental dynamics and mechanistic control of oocyte production from early progenitors have remained a mystery.

Our work uncovers previously unrecognized ovarian modules in zebrafish and human ovaries that serve as the developmental microenvironment for oocyte production from GSCs. We characterize the morphological organization of modules, resolve their developmental dynamics, recapitulate their architecture transcriptomically, and identify the mechanistic control of GSCs by Notch signaling. We show that GSCs at the young tip of modules give rise to oogonia and early differentiating oocytes, which then progress developmentally and linearly along the module before forming primordial follicles (Extended Data Fig. 7a). Altogether, our findings introduce a new concept in vertebrate female GSC biology that revises our understanding of early oogenesis and female reproduction. Our work supports a model of stem cell regulation and tissue morphogenesis in the ovary, outlined below.

Several lines of evidence suggest a dynamic view of development within modules. As a simple model for linear development in modules, we propose that *nos2*+ GSCs produce *foxl2l*+ progeny (either directly or indirectly through yet unidentified intermediate progenitors) and that *foxl2l*+ cells generate cysts. These cysts are likely pushed forward by newly born cells and newly formed cysts and, in parallel, progress linearly through developmental stages. Indeed, in addition to progressing gene expression patterns along modules, we observe transitioning cells that co-express consecutive developmental markers (Extended Data Fig. 1), as well as cyst sister cells connected by CBs but expressing distinct, sequential developmental markers (Fig. 1 and Supplementary Videos 4-5). These observations indicate that a cell's developmental state correlates with its position along the module rather than solely with its clonal cyst, supporting a higher-order organization within modules. Tight but dynamic spatiotemporal regulation along modules is likely required, but remains to be uncovered (discussed below).

Further, several lines of evidence suggest clonal dynamics underlying these developmental trajectories. First, we detected the presence of ≥2 lineages of GSC-to-developing oocyte clones within modules, arising from GSCs at the young tip (Fig. 3 and Extended Data 3). Second, we identified coexisting actively dividing and non-dividing GSCs at the young tip of modules (Extended Data Fig. 1). Third, we demonstrate the non-synchronous cell divisions of GSC-derived oogonial progeny (Fig. 3, Extended Data 3 and Supplementary Video 6-9). Based on these observations, we speculate that different GSC clones may in parallel and/or in an alternate manner produce *foxl2l*+ progeny that give rise to oogonial cysts (Extended Data Fig.

7b). These clonally independent cysts then progress linearly through meiotic stages within modules, as described above.

Mechanistically, we demonstrate GSC regulation by Notch signaling in modules (Extended Data Fig. 7c). After careful optimization of experimental conditions, we were able to recapitulate the module architecture on the transcriptomic level, and identify potential regulators of GSC differentiation in a data-driven manner, including the Notch signaling pathway. We establish that the Notch signaling pathway regulates GSCs and their production of oocytes by suppressing the *nos2*+ GSC fate and promoting the production of *foxl2l*+ progeny, followed by oocyte differentiation (Extended Data Fig. 7c). Based on our mapping of Notch pathway components in modules and our functional manipulation of Notch signaling, we hypothesize that *nos2*+ cells express the *Jag2b* ligand and maintain their GSC fate. We reason that, at some point, expression of *Notch2* and/or *Notch3* receptors is induced in a subset of *nos2*+ cells or in a yet unidentified intermediate progenitor. Once receptor(s) are expressed, these cells become competent to respond to Jag2b and activate Notch signaling, which then directs their fate as *foxl2l*+ progeny and promotes differentiation. Notch signaling may be required to repress GSC gene expression, activate progeny gene expression, or both. What induces the expression of *Notch2/3* receptors - and whether this is initiated stochastically or triggered by signals from neighboring cells (e.g., somatic cells) within modules - remains to be determined.

Additionally, more indirect regulation is also plausible through cross-talk between *nos2*+ GSCs and *Notch2* in somatic cells (Fig. 5d). In *Drosophila* and *C. elegans*, Notch signaling is required for the maintenance and function of niche cells[75,76,77,78,79,80], thereby indirectly regulating GSCs. A better understanding of the potentially different somatic cell types present along modules, including those that may function as niche cells, is needed to resolve their specific contributions to GSC regulation and oocyte production.

We have previously shown that NOTCH signaling is important for the formation of primordial follicles in humans with (JAG1+DLL3+) diplotene oocytes signaling to (NOTCH3+) granulosa cells[72]. This ligand-receptor interaction facilitates the attraction and organization of the granulosa cells around the oocyte, ultimately leading to the formation of primordial follicles. Here, we demonstrate that NOTCH signaling is also important for meiotic entry, with early germ cells signaling to RA-responsive germ cells at meiotic onset. Interestingly, this early regulation by

NOTCH signaling is likely conserved in species that show asynchronous germ cell development, whereby spatial distribution is important to regulate meiotic progression.

The Notch pathway is well established in the regulation of stem cells across various organ systems, e.g., in the zebrafish brain[81,82,83] (*81-83*). In most cases, Notch receptors are expressed in stem or progenitor cells, and pathway activity functions to maintain their undifferentiated state[81]. Interestingly, in zebrafish ovaries, and likely in human ovaries, Notch functions in the opposite manner, suppressing the *nos2*+ stem cell fate and promoting differentiation. This distinct mode of Notch function may reflect differences in the specific target genes regulated by the pathway in each context. In any case, beyond Notch, it is very likely that additional factors are required to maintain GSCs in ovaries. Overall, our data uncover previously unknown mechanistic principles underlying the developmental regulation of vertebrate female GSCs and their production of oocytes via the Notch signaling pathway in modules.

The organization of oocytes and early progenitors in modules may provide a platform for efficient developmental regulation. The ovarian modules we report here in zebrafish and human ovaries are, in principle, similar to the developmental organization of ovarioles in *Drosophila* and the gonad arm in *C. elegans*[69,70], and a comparable arrangement has also been observed in Medaka fish[24]. While major species-specific differences clearly exist among these animals, in all cases, GSCs and their oocyte progeny are spatially organized and regulated. The widespread use of this organizational principle across worms, insects, and vertebrates suggests a highly efficient developmental strategy that effectively balances GSC maintenance with oocyte production, both during development and in homeostasis. A linear progression of differentiation trajectories from spatially localized stem cells is a common principle in many tissues, and we now show that early oogenesis in the ovary follows a similar developmental rationale.

The discovery of ovarian modules offers a new paradigm and a revised view of oogenesis, raising many compelling questions. Two major directions for future investigation emerge. The first involves identification of distinct GSC subpopulations and development of tools to enable their live time-lapse imaging. Such tools will be instrumental in determining GSC division rates, assessing potential asymmetric divisions, and investigating their interactions with putative niche cells.

Elucidating the dynamics of GSCs at the young tip of modules at single-cell resolution is key. Throughout our analyses, we detected a minority of cells not adjacent to those at the immediate preceding stage. We hypothesize that this may reflect a finite half-life of GSCs at the young tip of modules, which in turn limits module lifespan. If GSCs at the young tip of modules ultimately decay, *foxl2l*+ clusters could appear isolated, followed by subsequently isolated *rec8*+ clusters as *foxl2l*+ progenitors are not replenished. We also observed solitary *nos2*+ cells/clusters outside modules. These may potentially represent a long-lived GSC pool. It is possible that from this reservoir, shorter-lived *nos2*+ cells could be recruited to form modules. This model is supported by our evidence for *nos2*+ sub-populations (Extended Data Fig. 1) and by reports of long- and short-lived GSCs in Medaka ovaries[24] and mouse testes[26,27]. Our transcriptomic analysis identified *kmt2b* and *dnmt3b* in *nos2*+ GSCs (Fig. 4 and Extended Data Table 4), which encode for regulators of stem cell-to-progenitor transitions[63,64,65], and potentially mark a developmentally advanced *nos2*+ sub-population. Future studies of these regulators, and of individual GSC dynamics at the module tip will help resolve these possibilities.

The second direction concerns potential higher-order spatial-temporal developmental regulation along modules. Progression through stages within modules is very likely governed by cell–cell interactions. These may include germ–germ cell interactions, such as those we identified between *nos2*+ and *foxl2l*+ cells via Notch signaling. Additionally, somatic–germ cell interactions may play key roles. It is tempting to speculate that somatic cells are spatially patterned and differentially express developmental cues along modules to control oocyte progression. Supporting this view, our single-cell transcriptomic analysis identified four related clusters of somatic cells that may exert stage-specific influences. A major future effort will be to identify and test specific spatial regulation by distinct somatic cell types along modules that may coordinate germ cell development. Thus, beyond the new concept of ovarian modules uncovered here, our work lays the foundation for establishing further paradigms in stem cell biology and reproduction.

Finally, by addressing a long-sought fundamental question in developmental biology, our findings may contribute to advancing female reproductive medicine. The conservation of the newly identified mode of oogenesis from GSCs and through modules between zebrafish and humans is striking. However, while zebrafish maintain GSCs throughout life, in humans their maintenance is limited to the first 35 weeks of pregnancy. Therefore, as we show here for Notch signaling, identifying regulators of GSCs and their production of oocytes in zebrafish holds great

potential for uncovering the missing factor(s) required for GSC maintenance in women. Overall, our work lays a foundation for future advances in female reproductive regenerative medicine.

Methods

Ethics statement

Zebrafish experiments were supervised by the Hebrew University Authority for Biological Models according to the institutional animal care and use committee and accredited by AAALAC. All experiments were appropriately approved under ethics requests MD-24-17017-1, md-20-16228-4, and MD-2024-17553-1. Zebrafish were bred, raised and maintained in accordance with the FELASA guidelines[78], the guidelines of the Max Delbrück Center for Molecular Medicine and the Helmholtz Center Munich, and the local authorities for animal protection (Landesamt für Gesundheit und Soziales, Berlin, and Regierung von Oberbayern, Munich, Germany) for the use of laboratory animals, based on the current version of German law on the protection of animals and EU directive 2010/63/EU on the protection of animals used for scientific purposes.

The use of with human material in this study adhered to the Declaration of Helsinki for Medical Research involving Human Subjects. A letter of no objection from the Medical Ethical Committee of the Leiden University Medical Center was obtained (P08.087 and B21.052). The human fetal material was donated for scientific research with written informed consent from donors undergoing elective abortion (without medical indication). The developmental age of the fetal samples was estimated by ultrasonography.

Fish lines and gonad collection

Juvenile ovaries were collected from 4-6 week post-fertilization (wpf) juvenile fish. Fish had a standard length (SL) measured according to[79] and were consistently ~8-12mm. Ovary collection was done as in[28]. Briefly, to fix the ovaries for immunostaining, fish were cut along the ventral midline and the lateral body wall was removed. The head and tail were removed and the trunk pieces, with the exposed abdomen containing the ovaries, were fixed in 4% PFA at 4°C overnight with nutation. Trunks were then washed in PBS and ovaries were finely dissected in cold PBS. Ovaries were washed in PBS and then either stored in PBS at 4°C in the dark, or dehydrated and stored in 100% MeOH at -20°C in the dark. Fish lines used in this research are:

Tü and AB wt, *Tg(b-act:Zebrabow)*[43], *Tg(b–act: mCherry-Cep55l)*[30], *Tg(b-act:loxp-STOP-loxp-hmgb1-mCherry)*[51], *Tg(hsp70l:Cre-ERT2)*[52], and *Tg(h2a:H2A-GFP)*[80].

Genotyping

Genotyping was performed at 4-5 wpf and over maximum of 2 days, after which fish were rested and raised in the system for at least a week until the collection of their ovaries at 5-7 wpf. Fish were anaesthetized in 0.02% Tricaine (Sigma Aldrich, #A5040) in system water, and a piece of their fin tail was clipped for DNA extraction. DNA was extracted using the standard *HotSHOT* DNA preparation method. *Tg(bAc:loxp-STOP-loxp-hmgb1-mCherry)* and *Tg(hsp70l:Cre-ERT2)* fish were genotyped by genomic PCR, using PCRBIO HS Taq Mix Red (PCR Biosystems #PB10.13-02), with the following primers: forward: AAGGGCGAGGAGGACAAC, GGCCACTAAACATGCTTCA, respectively, and reverse: ATGAACTGAGGGGACAGGA, ACACCAGAGACGGAAATCCATC, respectively.

Immunofluorescence (IF) and HCR-FISH

Fluorescence immunohistochemistry was performed as in[28]. Briefly, ovaries were washed 4 x 20 minutes in PBT (0.3% Triton X-100 in 1xPBS. If stored in MeOH, ovaries were gradually rehydrated before washes. Ovaries were blocked for 1.5-2 hours in blocking solution (10% FBS in PBT) at room temperature, and then incubated with primary antibodies in blocking solution at 4°C overnight. Ovaries were washed 4 x 20 minutes in PBT and incubated with secondary antibodies in fresh blocking solution for 2 hours, and were light protected from this step onward. Ovaries were then washed 4 x 20 minutes in PBT and incubated in PBT containing DAPI (1:1000, Molecular Probes), with or without DiOC6 (1:5000, Molecular Probes) for 50 minutes and washed 2 x 5 minutes in PBT and 2 x 5 minutes in PBS. Ovaries were mounted in Vectashield (with DAPI, Vector Labs) between two #1.5 coverslips using a 120µm spacer (Molecular Probes).

Primary antibodies used were Ddx4 (1:5,000)(*81*), β-catenin (1:1,000, Sigma-Aldrich), anti-mCherry (1:250, Abcam), pHH3 (1:200, Sigma-Aldrich). Secondary antibodies used were Alexa Fluor 488 and 594 (1:500; Molecular Probes). Vital dyes used were: DiOC6 (1:5000, Molecular Probes).

HCR-FISH was performed according to the manufacturer protocol (Molecular Instruments) and was adjusted for ovaries as in[32]. Briefly, ovaries were rehydrated and washed 5 x 5 min and 3 x 20 min with PBST. Ovaries were then washed 5 min with probe hybridization buffer at RT and pre-hybridized with 100 µl probe hybridization buffer for 30 min at 37^0, followed by hybridization with probes of interest for O.N at 37^{0}C. Ovaries were washed 4 x 15 min with probe wash buffer at 37^{0}C and then 3 x 15 min with 5X SSCT at RT. Ovaries were incubated in pre-amplification buffer for 30 min at RT, and then for O.N (in the dark) at RT with amplifying solution containing hairpins. Ovaries were washed 5 x SSCT for 2 x 5 min, 2 x 30 min, and 1 x min, and counterstained for DAPI and DIOC6 and mounted as described in ProLong Gold antifade mounting media (Invitrogen, P10144). Probes used: zebrafish probes: *nanos2, foxl2l, rec8a, dmc1*, *jag2b, notch2, notch3* and *her6.* Human probes: *Stra8*, *Sycp3*.

Human tissue sample preparation

Fetal ovaries from 19WG from different donors were isolated, embedded in 4% low melting point agarose (V2111, Promega) and cut into 200 µm-thick slices using a vibratome (vt1200 S, Leica). Thereafter, the tissue slices were fixed in 4% paraformaldehyde (PFA) for 20 minutes (min) at room temperature (RT), washed several times in 1x phosphate-buffered solution (PBS) and stored either in PBS at 4°C for whole mount immunofluorescence of in 100% methanol at -20C for HCR-FISH.

Whole mount immunofluorescence on human tissue slices

Tissue slices were permeabilized for 30 min in 0.3% TritonX-100 (Sigma-Aldrich) in 1x PBS and incubated with primary antibodies diluted in blocking buffer [1% bovine serum albumin (10735086001, Roche) + 1% TritonX-100 and 0.1% saponin (47036, Sigma-Aldrich Chemie) in PBS] at 37°C for 4 days with mild agitation (Eppendorf Thermomixer). Primary antibodies used were mouse anti-TRF1/2 (ab10579, Abcam, 1:100), mouse anti-POU5F1 (sc-5279, Santa Cruz, 1:200), goat anti-SYCP3 (AF3750, R&D Systems, 1:500), rabbit anti-DDX4 (ab13840, Abcam, 1:500), goat anti-DDX4 (AF2030, R&D Systems, 1:1000), rabbit anti-NOTCH2 (5732T, Cell Signaling, 1:200). Thereafter, the tissue slices were washed with 0.2% TritonX-100 in PBS 6x 30min, followed by incubation with secondary antibodies and DAPI (4′,6-diamidino-2-phenylindole, D3571, Life Technologies, 1:1000) diluted in blocking buffer for 2 days and washed with 0.2% TritonX-100 in PBS 6x 30min at seps at RT with rotation. Secondary antibodies used

were donkey anti-mouse 488 (A21202, Invitrogen, 1:500), donkey anti-goat 594 (A-11058, Invitrogen, 1:500) and donkey anti-rabbit 647 (Invitrogen, A-31573, 1:500). Afterwards, the tissue slices were transferred to individual µ-Slide 18 wells (81816, IBIDI) for confocal microscopy.

Confocal microscopy

Images were acquired on a Zeiss LSM 880 confocal microscope using a 40× lens. The acquisition setting was set across samples and experiments to: XY resolution = 1104 × 1104 pixels, 12-bit, 2× sampling averaging, pixel dwell time = 0.59 s, zoom = 0.8×, pinhole adjusted to 1.1 µm of Z thickness. Increments between images in stacks were 0.53µm, and laser power and gain were set in an antibody-dependent manner to 7 to 11% and 400 to 650, respectively, below saturation condition. Unless otherwise noted, images shown are partial sum Z-projection. Acquired images were not manipulated and only contrast and brightness were linearly adjusted. All figures were made using Adobe Photoshop CC 2014.

Human tissue slices were scanned as above or using an inverted Andor Dragonfly 200 with spinning disk (Oxford instruments) with consistent parameters: 40x water immersion objective (NA 0.8), with automatic increments between images in stacks (0.53 µm). The acquisition setting was: XY resolution 2048 x 2046 pixels, 12-bit. All images were processed in Imaris (version 10.2.0).

Three-dimensional segmentation of confocal data

Z-stacks of raw 3-dimentional confocal microscopy images of entire modules were imported to IMARIS, and nuclei, membranes, HCR-FISH, and IF signals were segmented using blend volume rendering mode. Signal brightness and object transparency were slightly adjusted linearly to optimize signal visualization. Animation frames were made using the key frame animation tool and videos were exported as video files.

Three-dimensional segmentation of modules from SBF-SEM

SBF-SEM image datasets from[30] containing Z-stacks images of modules were manually segmented in IMARIS. Image voxel size was corrected, and cell membranes were traced in each individual Z section using manual volume rendering mode. Individual sections were reconstructed to create the surface of cells in 3D. Videos were created as described above.

Intensity measurements of marker gene HCR-FISH signals in modules

In confocal images of modules, HCR-FISH intensities were measured per marker gene and module in ImageJ. A measuring line was drawn along the module midline, and across the entire module length from the start to the end, and HCR-FISH signal intensity for a given marker gene was measured along the line using the plot profile tool. Intensity values were normalized in R studio for each channel, using the min-max normalization plug-in. Normalized values along distance of the measuring line were plotted in R studio.

Supervised segmentation of HCR-FISH signals in modules and Euclidean distance analysis

Confocal images of HCR-FISH labeled ovaries were segmented in 3D similar to[31], with the following modifications. A custom ImageJ macro script was used to pre-process the 3D image dataset (Extended Data Fig. 2)[82]. Pre-processing steps included removing noise and segmenting[83,84] the signal using Euclidean distance transform watershed. Manual correction of segmented labels and removal of unwanted labels was done using Napari, a Python-based program for visualization and analysis[85]. A custom Python script was developed to generate a pairwise label image of stage-specific clusters (based on HCR labels) from input images. The script will be made available publicly in GitHub (https://github.com/jb-kroll/zebrafish_ovarian_module/tree/main).

In the generated pairwise label image, one label is considered as reference, and the shortest Euclidean distance between the pair in 3D is calculated. 3D Euclidean distance was calculated using SciPy module's exact Euclidean distance transform function. The maximum threshold of 3D Euclidean distance to consider a label pair as adjacent was set at 15 pixels, which is approximately half the diameter of module cells in this space (based on the average of the sizes of GSCs, oogonia, leptotene, and zygotene cells). We reasoned that adjacent clusters interface one another and are thus found within less than one cell-diameter distance from each other, and therefore defined half a diameter as a conservative, strict criteria. Clusters with 3D Euclidean distance of $\leq$15 pixels were scored as "adjacent", and those with $>$15 pixels were scored as "not adjacent". The frequency of labeled stage specific clusters found to be adjacent and not adjacent was pooled and plotted as a relative frequency plot in GraphPad Prism.

Lineage-tracing

For lineage tracing experiments, 2.5 dpf *Tg(bAc:loxp-STOP-loxp-hmgb1-mCherry)*; *Tg(hsp70l:Cre-ERT2)* larvae were pulsed with a regime of heat-shock treatments and 4-hydroxy-tamoxifen (4-OHT) administration as described[53]. Briefly, larvae in E3 culture medium were preheated to 36^{0}C for 15 minutes, and 10 µM 4-OHT was added to the medium for 45 min at 36^{0}C. After treatment, larvae were washed 3x with fresh E3. mCherry+ larvae were observed as early as 48 hours post treatment (hpt), and larvae were raised in normal husbandry conditions to juvenile stages. These treatments induced sparce partial recombination in primordial germ cells, as detected at 6 dpf (PGCs; Methods and Extended Data Fig. 3a), and later in early developing ovaries in juvenile stages at 4-5 weeks post-fertilization (wpf), as detected by cells with mCherry+ nuclei (Extended Data Fig. 3b). To analyze mCherry+ lineages we labeled ovaries for mCherry combined with multiplexed HCR-FISH for GSC and oocyte developmental marker genes.

***Ex-vivo* ovary culture**

Ovaries were cultured as described in[34]. Briefly, 4-5 wpf ovaries were dissected in sterile conditions and plated on 35 mm glass bottom dish coated with poly-D-Lysine (PDL). Ovaries were cultured in complete ovary culture media 1 [COCM1; Dulbecco's modified Eagle's medium (DMEM) high glucose (Sartorius), containing: ovary extract, fetal bovine serum (FBS,10%, Sigma), HEPES Buffer Solution (20µm, gibco), L-alanyl-L-glutamine (2mM, sigma), penicillin/ streptomycin/ amphotericin b solution (1%, Sigma), Fish serum (1%, the serum of Oncorhynchus mykiss was bought form kibbutz Dan), Insulin-Transferrin-Selenium ITS (1%, Sigma), 1 ng/ml 17alpha, 20beta-dihydroxy-4-pregnen-3-one (DHP) (Cayman chemical #16146), and 1 ng/ml Estradiol-17 beta (E2) (Sigma Aldrich #E2758)]. Ovaries were cultured at 28°C and 5% CO2 atmosphere. For live time-lapse imaging ovaries were imaged starting 0 dpc, for small molecule inhibitor experiments DMSO or DAPT (Sigma Aldrich # D5942) were added to COCM1 at 1 dpc, and ovaries were collected at the end of treatment at 3 dpc.

Live time-lapse imaging

Cultured *Tg(h2a:H2A-GFP)* ovaries were imaged live starting at 0 dpc, in a Nikon Spinning disk confocal microscope with Ti2-ZDrive using a cage incubator set for 28°C and 5% CO2

atmosphere. Time-lapse Z-stack images were acquired over time with the following acquisition settings across experiments: XY resolution = 2304 x 2304 pixels, 16-bit – No Binning, 10% laser power, Z increments between images in stacks were 0.6 µm and time interval between images was 10 minutes, lens objectives used: 20x or 40x. Ovaries were imaged for a total time duration of up to 53 hours. Frames covering large portions of the ovary were recorded. Dividing cells were identified across the tissue at various timepoints. Fig. 3j, Extended Data Fig. 3d, and Supplementary Videos 6-9 show zoom-in ROIs of dividing cells in space and time.

Single cell dissociation of zebrafish ovaries for scRNA-seq with Parse Biosciences

All tubes were coated with 1% BSA in PBS. Ovaries from 30 AB fish at 5 wpf were dissected and incubated in HL-15 during dissections. The tissue was enzymatically dissociated in two steps. First a mix of 1.2 mg/ml Collagenase I, 1.2 mg/ml Collagenase II and 0.26 mg/ml Hyaluronidase in HBSS without Ca^{2+} and Mg^{2+} was added and incubated for 10 minutes at 37 ˚C. The ovaries were split into two dissociation reactions and each reaction had a total volume of 331 µl. The reaction was pipetted up and down every two minutes. After 10 minutes 400 µl of TriplE (1x with EDTA) was added and again incubated for 10 min at 37 ˚C. The reaction was stopped by adding 200 µl of 10% BSA in PBS. The mix was centrifuged at 300 g for 3 min at 4 ˚C, the supernatant was discarded and the cells resuspended in 500 µl HBSS. The cell mix was filtered with a 70 µm sieve and again centrifuged at 300 g for 3 min at 4 ˚C. The cell mix was inspected for doublets and 2% doublets were still observed. The supernatant was discarded and the cells were resuspended in the fixation buffer and filtered at 40 µm. The Evercode™ Cell Fixation v3 protocol was followed for fixation. The last centrifugation step in the Fixation protocol was carried out with 500 g for 5 min at 4 ˚C. The fixed cells were resuspended in 100 µl resuspension buffer. After fixation cells were counted with Trypan blue. 30% doublets were observed following the fixation. This doublet rate was later considered during the analysis.

Parse protocol and sequencing settings

Fixed cells were used immediately after fixation and not frozen in between. For library preparation the Parsebio Evercode WT Mini v3 kit was used and the protocol was followed as recommended. All centrifugation steps in the split&pool part were performed with 500 g for 5 min. In the final cell lysis step 7500 cells were lysed per sub-library.

The final library was sequenced with 800 Mio reads with Dual Index Sequencing on a NextSeq2000 with 5% PhiX.

Single cell dissociation for scRNA-seq with 10X Genomics

All tubes were coated with 1% BSA in PBS. Ovaries from 30 AB fish at 5 wpf were dissected and incubated in HL-15 during dissections. The tissue was enzymatically dissociated with a mix of 1.2 mg/ml Collagenase I, 1.2 mg/ml Collagenase II and 0.26 mg/ml Hyaluronidase in HBSS (Ca^{2+}-, Mg^{2+}-) for 20 minutes at 37 ˚C in a total volume of 662 µl. The reaction was mixed by a rotor for the duration of the dissociation. The reaction was stopped by adding 1.5 ml of buffer to dilute the enzymes. µl of 10% BSA in PBS. The mix was centrifuged at 300 g for 3 min at 4 ˚C, the supernatant was discarded and the cells resuspended in 500 µl HBSS. The cell mix was filtered with a 70 µm sieve and again centrifuged at 300 g for 3 min at 4 ˚C. The cells were finally resuspended in 60 µl HBSS (Ca^{2+}-, Mg^{2+}-) with 1% BSA and counted with Trypan blue.

10X Genomics protocol and sequencing settings

Cells were used immediately after counting for 10X Gene Expression library preparation. The Chromium Next GEM Single Cell 3' Reagent Kits v3.1 (Dual Index) protocol in the revised version E was followed. The final library was sequenced with 150 Mio reads with Dual Index Sequencing on a NextSeq2000 with 10% PhiX.

Cellranger & ParseBio pipeline.

Raw sequencing files were demultiplexed using bcl2fastq with standard settings and then the respective pipelines were run for creating cellxgenes matrices. For Parsebio data the split-pipe pipeline version 1.2.1 was used and mapped to the dr11 genome.

For 10X GEX data cellranger version 7.1.0. was used and it was mapped to the dr11 genome without including introns. Mapping resulted in a warning message for "Low Fraction Reads in Cells", possibly caused by high levels for ambient RNA.

Preprocessing pipeline

Seurat Version 5.1.0. and R Version 4.4.1 was used for obtaining a cleaned clustered dataset. All cells were processed in a first step, without removing low quality cells or putative doublets identified by high counts (Extended Data Fig. 4a). In all cells, expression per cell was normalized using SCTransform from Seurat (https://doi.org/10.1186/s13059-019-1874-1). Principal component analysis (PCA) was performed with variable features, the top 25 PCs were retained, and a k-nearest neighbor (kNN) graph was constructed using top components. Clustering was performed using the Leiden algorithm at resolution 0.5. Results were visualized with Uniform Manifold Approximation and Projection (UMAP). The expression of *ddx4*, *gsdf* and *col1a1a* were used to distinguish between oocytes and other cell types, and the dataset was split into two subsets of oocytes and "other cell types" (Extended Data Fig. 4b, c). The "other cell types" were filtered in two steps. First, regular quality cutoffs were applied and cells with over 5000 genes and 50,000 transcripts were removed (Extended Data Fig. 4d, e). Additionally, an oocyte score with *ddx4* and *piwi1* and a late-oocyte score with *zp3.2* and *zp3b* were calculated , and cells scoring over 0.5 (oocyte_score) and over 0.0 (late_oocyte_score) were removed (Extended Data Fig. 4f, g). This was to ensure that all doublets between oocytes and other cell types are removed. The oocyte subcluster was inspected and a quality cutoff for high transcript counts was set to 100,000 (Extended Data Fig. 4h, i). The oocytes subcluster was again processed as described above, and clusters with expression of marker genes typical for other cell types were removed (Extended Data Fig. 4k, j). The subsets of oocytes and other cell types were combined again and processed for clustering. Cell types were annotated using known marker gene expression per cluster. Marker genes per cell type were calculated with the Seurat function FindallMarkers() and min.pct = 0.25, logfc.threshold = 0.25 arguments. The 10X data were processed with the same steps although different cutoffs were applied (Extended Data Fig. 5).

Subclustering, pseudotime calculation and marker gene correlation

For sub-clustering the clusters expressing *ddx4* were subsetted and newly clustered using SCTransform, PCA (20) and the kNN graph. Clustering was performed using the Leiden algorithm at resolution 0.6. Results were visualized by UMAP. Markers were calculated with the Seurat function FindallMarkers() and min.pct = 0.25, logfc.threshold = 0.25 arguments. This clustering was used for pseudotime construction using SCORPIUS (doi:10.1101/079509), UMAP

coordinates were extracted and a trajectory was inferred with k=3. The trajectory was reversed to set the start to the *nanos2* cluster. Expression of marker genes was plotted over pseudotime using the normalized expression values calculated with SCTransform.

To find genes with similar expression patterns over pseudotime, gene expression was correlated to marker gene expression. After isolating the relevant subset of cells representing the early trajectory stages (based on UMAP clustering and pseudotime inference), the normalized expression matrix was extracted and *nanos2*, *foxl2l*, *rec8a* and *dcm1* were used as a reference vector. The Spearman rank correlation coefficient (ρ) was computed between the expression of each gene and the expression profiles of the marker genes across all cells in the subset. This was performed using the cor.test() function in R. To control for multiple testing, all p-values were adjusted using the Benjamini–Hochberg procedure. Genes were then ranked by their correlation coefficients, and the top positively correlated genes were selected for visualization and downstream analysis. These genes were plotted across pseudotime using smoothed LOESS regression to visualize their dynamic expression profiles relative to the marker genes. This allowed us to find dynamic, more nuanced changes over pseudotime rather than merely identifying genes that increase or decrease in a monotonic fashion.

RNA-seq analysis of single-cell transcriptomics of human fetal ovaries

Online-available single-cell transcriptomics data from human fetal ovaries 18-26WG were obtained from Gene Expression Omnibus (GEO) with accession number GSE106487[72]. Data curation and cluster identity was performed as previously described[69]. The dataset was analyzed using a Seurat-based workflow (v4.3.0.1)[86] using R (v4.3.3.). t-SNE plots showing cell cluster identity and age were generated using Seurat function DimPlot. The per cluster average gene expression was calculated using a custom R script. Genes of interest were selected and their expression values were visualized on a heatmap using heatmap.2 function from R package ggplots (v3.1.3).

Statistical analysis

All statistical analysis and data plotting were performed using GraphPad Prism 7 software. Datasets were tested with two way ANOVA. In the figures, *P* values are indicated by

asterisks as follows: *$P < 0.05$, **$P < 0.01$, ***$P < 0.001$, and ****$P < 0.0001$ (ns, not significant at $P > 0.05$).

References

1. D. G. de Rooij, The nature and dynamics of spermatogonial stem cells. *Development* **144**, 3022–3030 (2017).
2. T. Lord, J. M. Oatley, A revised Asingle model to explain stem cell dynamics in the mouse male germline. *Reproduction* **154**, R55–R64 (2017).
3. D. Drummond-Barbosa, Local and Physiological Control of Germline Stem Cell Lineages in Drosophila melanogaster. *Genetics* **213**, 9–26 (2019).
4. S. J. Morrison, A. C. Spradling, Stem cells and niches: mechanisms that promote stem cell maintenance throughout life. *Cell* **132**, 598–611 (2008).
5. B. J. Lesch, D. C. Page, Genetics of germ cell development. *Nat Rev Genet* **13**, 781–794 (2012).
6. Y. Kim *et al.*, Fgf9 and Wnt4 act as antagonistic signals to regulate mammalian sex determination. *PLoS Biol* **4**, e187 (2006).
7. J. Bowles *et al.*, FGF9 suppresses meiosis and promotes male germ cell fate in mice. *Dev Cell* **19**, 440–449 (2010).
8. J. S. Colvin, R. P. Green, J. Schmahl, B. Capel, D. M. Ornitz, Male-to-female sex reversal in mice lacking fibroblast growth factor 9. *Cell* **104**, 875–889 (2001).
9. L. DiNapoli, J. Batchvarov, B. Capel, FGF9 promotes survival of germ cells in the fetal testis. *Development* **133**, 1519–1527 (2006).
10. J. Johnson, J. Canning, T. Kaneko, J. K. Pru, J. L. Tilly, Germline stem cells and follicular renewal in the postnatal mammalian ovary. *Nature* **428**, 145–150 (2004).
11. Y. A. R. White *et al.*, Oocyte formation by mitotically active germ cells purified from ovaries of reproductive-age women. *Nature Medicine* **18**, 413–421 (2012).
12. J. J. Martin, D. C. Woods, J. L. Tilly, Implications and Current Limitations of Oogenesis from Female Germline or Oogonial Stem Cells in Adult Mammalian Ovaries. *Cells* **8**, (2019).
13. R. A. Anderson, N. Fulton, G. Cowan, S. Coutts, P. T. K. Saunders, Conserved and divergent patterns of expression of DAZL, VASA and OCT4 in the germ cells of the human fetal ovary and testis. *BMC developmental biology* **7**, 136 (2007).

14. D. Farini, M. De Felici, The Beginning of Meiosis in Mammalian Female Germ Cells: A Never-Ending Story of Intrinsic and Extrinsic Factors. *International Journal of Molecular Sciences* **23**, 12571 (2022).
15. L. F. Kurilo, Oogenesis in antenatal development in man. *Human Genetics* **57**, 86–92 (1981).
16. Y. M. Elkouby, M. C. Mullins, Coordination of cellular differentiation, polarity, mitosis and meiosis - New findings from early vertebrate oogenesis. *Dev Biol* **430**, 275–287 (2017).
17. R. L. Beer, B. W. Draper, nanos3 maintains germline stem cells and expression of the conserved germline stem cell gene nanos2 in the zebrafish ovary. *Dev Biol* **374**, 308–318 (2013).
18. Z. Cao, X. Mao, L. Luo, Germline Stem Cells Drive Ovary Regeneration in Zebrafish. *Cell reports* **26**, 1709–1717 e1703 (2019).
19. F. Barrios *et al.*, Opposing effects of retinoic acid and FGF9 on Nanos2 expression and meiotic entry of mouse germ cells. *J Cell Sci* **123**, 871–880 (2010).
20. A. Suzuki, K. Igarashi, K. Aisaki, J. Kanno, Y. Saga, NANOS2 interacts with the CCR4-NOT deadenylation complex and leads to suppression of specific RNAs. *Proc Natl Acad Sci U S A* **107**, 3594–3599 (2010).
21. A. Suzuki, Y. Saga, Nanos2 suppresses meiosis and promotes male germ cell differentiation. *Genes Dev* **22**, 430–435 (2008).
22. M. Tsuda *et al.*, Conserved role of nanos proteins in germ cell development. *Science* **301**, 1239–1241 (2003).
23. K. M. Kusz *et al.*, The highly conserved NANOS2 protein: testis-specific expression and significance for the human male reproduction. *MHR: Basic science of reproductive medicine* **15**, 165–171 (2009).
24. S. Nakamura, K. Kobayashi, T. Nishimura, S. Higashijima, M. Tanaka, Identification of germline stem cells in the ovary of the teleost medaka. *Science* **328**, 1561–1563 (2010).
25. A. Suzuki, M. Tsuda, Y. Saga, Functional redundancy among Nanos proteins and a distinct role of Nanos2 during male germ cell development. *Development* **134**, 77–83 (2007).

26. T. Nakagawa, Y. Nabeshima, S. Yoshida, Functional identification of the actual and potential stem cell compartments in mouse spermatogenesis. *Dev Cell* **12**, 195–206 (2007).
27. A. Sada, A. Suzuki, H. Suzuki, Y. Saga, The RNA-Binding Protein NANOS2 Is Required to Maintain Murine Spermatogonial Stem Cells. *Science* **325**, 1394–1398 (2009).
28. Y. M. Elkouby, M. C. Mullins, Methods for the analysis of early oogenesis in Zebrafish. *Dev Biol* **430**, 310–324 (2017).
29. Y. Bogoch *et al.*, Stage Specific Transcriptomic Analysis and Database for Zebrafish Oogenesis. *Front Cell Dev Biol* **10**, 826892 (2022).
30. A. Mytlis *et al.*, Control of meiotic chromosomal bouquet and germ cell morphogenesis by the zygotene cilium. *Science* **376**, eabh3104 (2022).
31. V. Kumar, Y. M. Elkouby, Tools to analyze the organization and formation of the germline cyst in zebrafish oogenesis. *Development* **150**, (2023).
32. A. Ahmad *et al.*, The piRNA protein Asz1 is essential for germ cell and gonad development in zebrafish and exhibits differential necessities in distinct types of germ granules. *PLoS Genet* **21**, e1010868 (2025).
33. S. Kar *et al.*, The Balbiani body is formed by microtubule-controlled molecular condensation of Buc in early oogenesis. *Curr Biol* **35**, 315–332.e317 (2025).
34. A. Shawahny, Y. Bogoch, Y. M. Elkouby, A Novel mTOR-Stat3-Stathmin Pathway Establishes Oocyte Polarization Competence by Orchestrating Centrosome Regulation and Microtubule Organization. *bioRxiv*, 2025.2002.2027.640508 (2025).
35. F. L. Marlow, M. C. Mullins, Bucky ball functions in Balbiani body assembly and animal-vegetal polarity in the oocyte and follicle cell layer in zebrafish. *Dev Biol* **321**, 40–50 (2008).
36. D. H. Leu, B. W. Draper, The ziwi promoter drives germline-specific gene expression in zebrafish. *Dev Dyn* **239**, 2714–2721 (2010).
37. Y. M. Elkouby, A. Jamieson-Lucy, M. C. Mullins, Oocyte Polarization Is Coupled to the Chromosomal Bouquet, a Conserved Polarized Nuclear Configuration in Meiosis. *PLoS Biol* **14**, e1002335 (2016).
38. M. P. Greenbaum, N. Iwamori, J. E. Agno, M. M. Matzuk, Mouse TEX14 is required for embryonic germ cell intercellular bridges but not female fertility. *Biol Reprod* **80**, 449–457 (2009).

39. W. Niu, A. C. Spradling, Mouse oocytes develop in cysts with the help of nurse cells. *Cell* **185**, 2576–2590.e2512 (2022).

40. M. E. Pepling, A. C. Spradling, Female mouse germ cells form synchronously dividing cysts. *Development* **125**, 3323–3328 (1998).

41. L. Lei, A. C. Spradling, Mouse primordial germ cells produce cysts that partially fragment prior to meiosis. *Development* **140**, 2075–2081 (2013).

42. L. Lei, A. C. Spradling, Mouse oocytes differentiate through organelle enrichment from sister cyst germ cells. *Science* **352**, 95–99 (2016).

43. Y. A. Pan *et al.*, Zebrabow: multispectral cell labeling for cell tracing and lineage analysis in zebrafish. *Development* **140**, 2835–2846 (2013).

44. C. H. Yang, Y. W. Wang, C. W. Hsu, B. C. Chung, Zebrafish Foxl2l functions in proliferating germ cells for female meiotic entry. *Dev Biol* **517**, 91–99 (2025).

45. Y. Liu *et al.*, Single-cell transcriptome reveals insights into the development and function of the zebrafish ovary. *Elife* **11**, (2022).

46. M. P. Greenbaum, L. Ma, M. M. Matzuk, Conversion of midbodies into germ cell intercellular bridges. *Dev Biol* **305**, 389–396 (2007).

47. Y. Elkouby, M. Mullins, Methods for the analysis of early oogenesis in zebrafish. *Developmental biology* **430**, 310–324 (2017).

48. Z. Cao, X. Mao, L. Luo, Germline Stem Cells Drive Ovary Regeneration in Zebrafish. *Cell Rep* **26**, 1709–1717.e1703 (2019).

49. C. L. Sansam, R. J. Pezza, Connecting by breaking and repairing: mechanisms of DNA strand exchange in meiotic recombination. *Febs j* **282**, 2444–2457 (2015).

50. Y. P. Blokhina, A. D. Nguyen, B. W. Draper, S. M. Burgess, The telomere bouquet is a hub where meiotic double-strand breaks, synapsis, and stable homolog juxtaposition are coordinated in the zebrafish, Danio rerio. *PLoS Genet* **15**, e1007730 (2019).

51. Y. Wang, M. Rovira, S. Yusuff, M. J. Parsons, Genetic inducible fate mapping in larval zebrafish reveals origins of adult insulin-producing β-cells. *Development* **138**, 609–617 (2011).

52. D. Hesselson, R. M. Anderson, M. Beinat, D. Y. Stainier, Distinct populations of quiescent and proliferative pancreatic beta-cells identified by HOTcre mediated labeling. *Proc Natl Acad Sci U S A* **106**, 14896–14901 (2009).

53. R. N. Das *et al.*, Generation of specialized blood vessels via lymphatic transdifferentiation. *Nature* **606**, 570–575 (2022).
54. E. W. Levy, I. Leite, B. W. Joyce, S. Y. Shvartsman, E. Posfai, A tug-of-war between germ cell motility and intercellular bridges controls germline cyst formation in mice. *Curr Biol* **34**, 5728–5738.e5724 (2024).
55. L. Deconinck, R. Cannoodt, W. Saelens, B. Deplancke, Y. Saeys, Recent advances in trajectory inference from single-cell omics data. *Current Opinion in Systems Biology* **27**, 100344 (2021).
56. C. W. Hsu *et al.*, Single cell transcriptomes of zebrafish germline reveal progenitor types and feminization by Foxl2l. *Elife* **14**, (2025).
57. E. Moses *et al.*, The killifish germline regulates longevity and somatic repair in a sex-specific manner. *Nat Aging* **4**, 791–813 (2024).
58. Q. Zhou *et al.*, Cross-organ single-cell transcriptome profiling reveals macrophage and dendritic cell heterogeneity in zebrafish. *Cell Rep* **42**, 112793 (2023).
59. G. Li *et al.*, Cebp1 and Cebpβ transcriptional axis controls eosinophilopoiesis in zebrafish. *Nat Commun* **15**, 811 (2024).
60. K. Ando *et al.*, Peri-arterial specification of vascular mural cells from naïve mesenchyme requires Notch signaling. *Development* **146**, (2019).
61. Y. Nagao *et al.*, Distinct interactions of Sox5 and Sox10 in fate specification of pigment cells in medaka and zebrafish. *PLoS Genet* **14**, e1007260 (2018).
62. R. J. Willms, L. O. Jones, J. C. Hocking, E. Foley, A cell atlas of microbe-responsive processes in the zebrafish intestine. *Cell Rep* **38**, 110311 (2022).
63. S. I. Tomizawa *et al.*, Kmt2b conveys monovalent and bivalent H3K4me3 in mouse spermatogonial stem cells at germline and embryonic promoters. *Development* **145**, (2018).
64. G. A. Challen *et al.*, Dnmt3a and Dnmt3b have overlapping and distinct functions in hematopoietic stem cells. *Cell Stem Cell* **15**, 350–364 (2014).
65. L. Rinaldi *et al.*, Dnmt3a and Dnmt3b Associate with Enhancers to Regulate Human Epidermal Stem Cell Homeostasis. *Cell Stem Cell* **19**, 491–501 (2016).
66. G. I. Uenishi *et al.*, NOTCH signaling specifies arterial-type definitive hemogenic endothelium from human pluripotent stem cells. *Nat Commun* **9**, 1828 (2018).

67. D. Sprinzak *et al.*, Cis-interactions between Notch and Delta generate mutually exclusive signalling states. *Nature* **465**, 86–90 (2010).
68. D. Sprinzak, S. C. Blacklow, Biophysics of Notch Signaling. *Annu Rev Biophys* **50**, 157–189 (2021).
69. R. Bastock, D. St Johnston, Drosophila oogenesis. *Curr Biol* **18**, R1082–1087 (2008).
70. N. Pazdernik, T. Schedl, Introduction to germ cell development in Caenorhabditis elegans. *Adv Exp Med Biol* **757**, 1–16 (2013).
71. X. Fan *et al.*, Transcriptional progression during meiotic prophase I reveals sex-specific features and X chromosome dynamics in human fetal female germline. *PLoS Genet* **17**, e1009773 (2021).
72. S. M. Czukiewska *et al.*, Cell-cell interactions during the formation of primordial follicles in humans. *Life Sci Alliance* **6**, (2023).
73. H. Shibuya, A. Morimoto, Y. Watanabe, The dissection of meiotic chromosome movement in mice using an in vivo electroporation technique. *PLoS Genet* **10**, e1004821 (2014).
74. L. Li *et al.*, Single-Cell RNA-Seq Analysis Maps Development of Human Germline Cells and Gonadal Niche Interactions. *Cell Stem Cell* **20**, 858–873.e854 (2017).
75. X. Song, G. B. Call, D. Kirilly, T. Xie, Notch signaling controls germline stem cell niche formation in the Drosophila ovary. *Development* **134**, 1071–1080 (2007).
76. E. J. Ward *et al.*, Stem cells signal to the niche through the Notch pathway in the Drosophila ovary. *Curr Biol* **16**, 2352–2358 (2006).
77. A. M. Zamfirescu, A. S. Yatsenko, H. R. Shcherbata, Notch signaling sculpts the stem cell niche. *Front Cell Dev Biol* **10**, 1027222 (2022).
78. E. J. A. Hubbard, T. Schedl, Biology of the Caenorhabditis elegans Germline Stem Cell System. *Genetics* **213**, 1145–1188 (2019).
79. D. Roy, D. J. Kahler, C. Yun, E. J. A. Hubbard, Functional Interactions Between rsks-1/S6K, glp-1/Notch, and Regulators of Caenorhabditis elegans Fertility and Germline Stem Cell Maintenance. *G3 (Bethesda)* **8**, 3293–3309 (2018).
80. S. L. Crittenden *et al.*, Sexual dimorphism of niche architecture and regulation of the Caenorhabditis elegans germline stem cell pool. *Mol Biol Cell* **30**, 1757–1769 (2019).
81. O. Gozlan, D. Sprinzak, Notch signaling in development and homeostasis. *Development* **150**, (2023).

82. P. Chapouton *et al.*, Notch activity levels control the balance between quiescence and recruitment of adult neural stem cells. *J Neurosci* **30**, 7961–7974 (2010).
83. T. Foley, M. Thetiot, L. Bally-Cuif, Neural Stem Cell Regulation in Zebrafish. *Annu Rev Genet* **58**, 249–272 (2024).
84. P. Aleström *et al.*, Zebrafish: Housing and husbandry recommendations. *Lab Anim* **54**, 213–224 (2020).
85. D. M. Parichy, M. R. Elizondo, M. G. Mills, T. N. Gordon, R. E. Engeszer, Normal table of postembryonic zebrafish development: staging by externally visible anatomy of the living fish. *Dev Dyn* **238**, 2975–3015 (2009).
86. S. Pauls, B. Geldmacher-Voss, J. A. Campos-Ortega, A zebrafish histone variant H2A.F/Z and a transgenic H2A.F/Z:GFP fusion protein for in vivo studies of embryonic development. *Dev Genes Evol* **211**, 603–610 (2001).
87. H. Knaut, F. Pelegri, K. Bohmann, H. Schwarz, C. Nüsslein-Volhard, Zebrafish vasa RNA but not its protein is a component of the germ plasm and segregates asymmetrically before germline specification. *J Cell Biol* **149**, 875–888 (2000).
88. C. A. Schneider, W. S. Rasband, K. W. Eliceiri, NIH Image to ImageJ: 25 years of image analysis. *Nat Methods* **9**, 671–675 (2012).
89. D. Legland, I. Arganda-Carreras, P. Andrey, MorphoLibJ: integrated library and plugins for mathematical morphology with ImageJ. *Bioinformatics* **32**, 3532–3534 (2016).
90. R. Haase *et al.*, CLIJ: GPU-accelerated image processing for everyone. *Nat Methods* **17**, 5–6 (2020).
91. N. Sofroniew *et al.*, napari: a multi-dimensional image viewer for Python. *Zenodo*, (2022).
92. Y. Hao *et al.*, Integrated analysis of multimodal single-cell data. *Cell* **184**, 3573–3587.e3529 (2021).

Acknowledgments

We are grateful to the Abisch-Frenkel Foundation Scholarship to NH, the Hebrew University International PhD Talent Scholarship to VK, the EMBO YIP support (#2023-5242) to YME, and the Novo Nordisk Foundation (reNEW NNF21CC0073729) to SMC and SMCdSL.

We would like to thank Albert Pen, Gil Levkowitz, and Karina Yaniv for the *zebrabow*, *Tg(bAc:loxp-STOP-loxp-hmgb1-mCherry)*, and *Tg(hsp70l:Cre-ERT2)* lines respectively, to Holger Knaut for the Ddx4 antibody, and to David Sprinzak for his valuable advice on Notch signaling. We thank Haley Grunloh (for Maayan Visuals) for graphical work. We thank Ronny Schäfer for help with zebrafish experiments, and Anika Neuschulz and Ioannis Moustakas for support with data analysis. We would further like to acknowledge support from the MDC/BIMSB genomics and zebrafish facilities. We are very grateful to the staff of the Vrelinghuis, Utrecht, for their efforts in obtaining the human fetal material, as well as the donors that have consented for the use of the material.

Funding

This work was funded by the Israel Science Foundation (ISF) grant #558/19, and Binational Science Foundation grant #2019263 to YME; and by the German Research Foundation (DFG) grant #540370162 to JPJ and YME; and the Novo Nordisk Foundation (reNEW NNF21CC0073729) to SMC and SMCdSL.

Author contributions

Conceptualization: NH, JBK, VK, SMCdSL, JPJ, and YME.

Methodology: NH, JBK, VK, SMC, NG, SMCdSL, JPJ, and YME.

Investigation: NH, JBK, VK, SMC, NG, YB, SMCdSL, JPJ, and YME.

Visualization: NH, JBK, VK, SMC, SMCdSL, and YME.

Formal Analysis: NH, JBK, VK, SMC, NG, YB, and SMCdSL.

Resources: YB, SMC, and SMCdSL.

Software: JBK, VK.

Funding acquisition: NH, JBK, VK, SMCdSL, JPJ, and YME.

Supervision: SMCdSL, JPJ, and YME.

Writing – original draft: NH, JBK, VK, SMC, SMCdSL, JPJ, and YME.

Competing interests

The authors have no competing interest.

Materials & Correspondence

All data are available in the manuscript or the supplementary materials. Material requests should be addressed to the corresponding author YME.

Figures and Figure legends

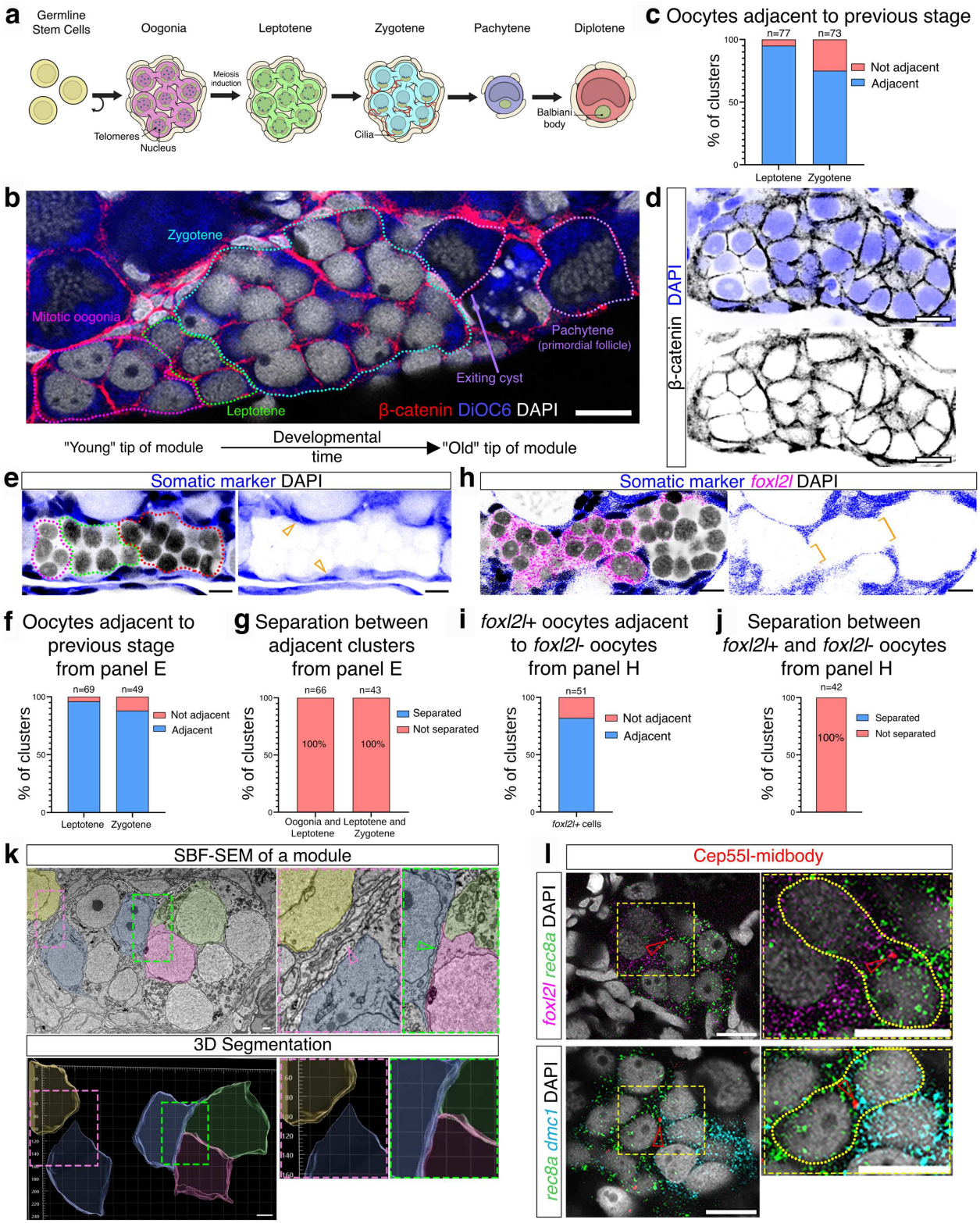

Figure 1. Newly identified ovarian modules. a. An outline of early oogenesis in zebrafish, including germline stem cells, mitotic oogonia and differentiating early oocytes within the

germline cyst, and pachytene and diplotene stages in primordial follicles. Distinct cellular features are shown along the developmental stages as indicated. **b-c.** A representative image of a module from whole ovaries labeled with β-catenin (red), DiOC6 (blue) and DAPI (grey). Clusters at specific stages are outlined color-coded as in a. The distribution of clusters adjacent or not adjacent to clusters at previous stages (leptotene to oogonia, and zygotene to leptotene) is plotted in c. n=number of clusters from 14 ovaries. **d.** Depiction of module morphology as labeled with β-catenin (black, inverted LUT) and DAPI (blue). **e.** Somatic cells (blue, yellow arrowheads) around modules are not detected between clusters at distinct developmental stages (outlined). Entire 3D stack is shown in Supplementary Video 1. The distribution of clusters adjacent or not adjacent to clusters at previous stages, which are collectively engulphed by somatic cells is plotted in **f**, and the distribution of adjacent clusters that are somatically separated or not separated from f is plotted in **g**. n=number of clusters from n=12 ovaries. **h.** Somatic cells (blue) around modules are not detected between *foxl2l*+ (magenta) clusters and *foxl2l*(-) clusters. Orange brackets indicate opening of somatic protrusions between clusters. Entire 3D stack is shown in Supplementary Video 2. The distribution of *foxl2l*+ clusters adjacent or not adjacent to *foxl2l* (-) clusters, which are collectively engulphed by somatic cells is plotted in **i**, and the distribution of adjacent *foxl2l*+ and *foxl2l* (-) clusters that are somatically separated or not separated from i is plotted in **j**. n=number of clusters from n=3 ovaries. **k.** SBF-SEM confirms lack of separation between adjacent stage-specific clusters in modules. Top: A single-section SBF-SEM image of leptotene and zygotene clusters in module. Oocytes are stages as in[28,30], where in brief, leptotene oocytes (i.e., blue colored oocytes) are smaller and exhibit nucleoli in the center of their nuclei, and zygotene cells (i.e., pink and yellow colored oocyte) are larger, with single peripheral nucleolus and visible tracks of presumptive synaptonemal complexes along chromosomes. Right panels are zoom-in images of color-coded boxes in left panel. Module cells are separated from outside cells by extra cell membranes (pink arrowhead), but membranes of leptotene and zygotene cells are interfaced (green arrowhead). Bottom: 3D reconstruction of colored segmented cells from single sections (top) confirms separation between module and non-module cells and lack of separation between module cells in 3D. Right panels are zoom-in images of color-coded boxes in left panel. Entire 3D stack and segmentation is shown in Supplementary Video 3. **l.** Oocytes at different stages are connected by CBs. Midbodies in CBs (mCherry-Cep55l, red, red arrowheads) are detected between *foxl2l*+ (magenta) and *rec8a*+ (green) cells (top), and between *rec8a*+ (green) and *dmc1*+ (cyan) cells (bottom). Right panels are zoom-in images of left panels. The cells at distinct stages that connected by CBs (red

arrowheads) are depicted (yellow outline). See also Supplementary Videos 4-5. n=6 ovaries for *foxl2l*+*rec8a* labeling, and 4 for *rec8*+*dmc1*. Scale bars in all panels are 10 μm.

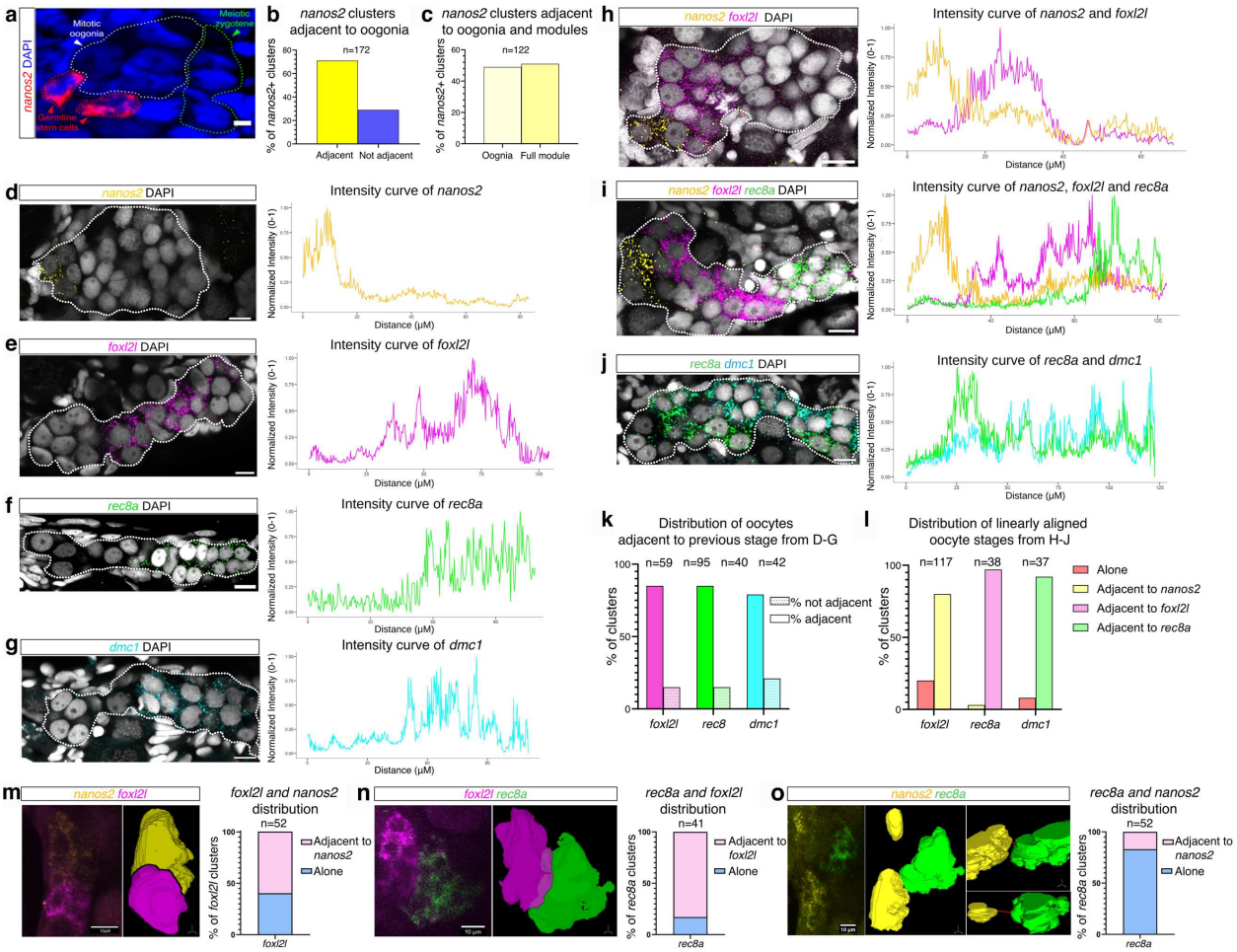

Figure 2. Expression patterns of developmental marker genes show spatial linear development of GSCs and oocytes in modules. a. GSCs are located at the young tip of modules. Ovaries labeled for *nos2* (red) and DAPI (blue), show *nos2*+ GSCs (red outline) are found next to modules containing oogonia (white outline) and meiotic stages (green outline). The distribution of *nos2*+ cells that are adjacent or not adjacent to oogonia is plotted in **b**, and the distribution of those from b that are adjacent to oogonia and full modules is plotted in **c**. n=number of clusters from 27 ovaries. See also Extended Data Fig. 1a-c. **d-g.** Representative images of developmental marker gene expression along modules (white outline), as indicated: *nos2* (yellow, d), *foxl2l* (magenta, e), *rec8a* (green, f), *dmc1 (*cyan, g). Right panels are representative normalized intensity plots of HCR-FISH signals along modules of the corresponding markers in the left panels. The distribution of oocyte clusters expressing a given marker, which are adjacent to clusters expressing an immediate preceding marker are plotted in **k**. n=number of clusters from 3-10 ovaries per probe. **h-j.** Representative expression pattern images and their corresponding normalized intensity plots along modules (white outline) as in d-

g, of multiplexed HCR-FISH probes for multiple markers, as indicated: *nos2* + *foxl2l* (h), *nos2* + *foxl2l* + *rec8* (i), *rec8* + *dmc1* (j). The distribution of oocyte clusters expressing a given marker, which are adjacent to clusters expressing an immediate preceding marker from multiplex experiments are plotted in **l**. n=number of clusters from 3 ovaries per probe combination. **m-o.** Raw sum-projection images of multiplexed markers (left) and their 3D automated segmentation (right) of stage specific clusters in our Euclidean distance analyses (Methods and Extended Data Fig. 2) are shown as indicated: *nos2* + *foxl2l* (m), *foxl2l* + *rec8* (n), *nos2* + *rec8* (o). The percentage of pairs that are scored as "adjacent" or "not adjacent" is plotted for each pair. The pair of *nos2* + *rec8* (o) serves as a control showing most developmentally non-consecutive clusters are not adjacent. n=number of clusters from 3 ovaries per probe combination. Scale bars in all panels are 10 μm.

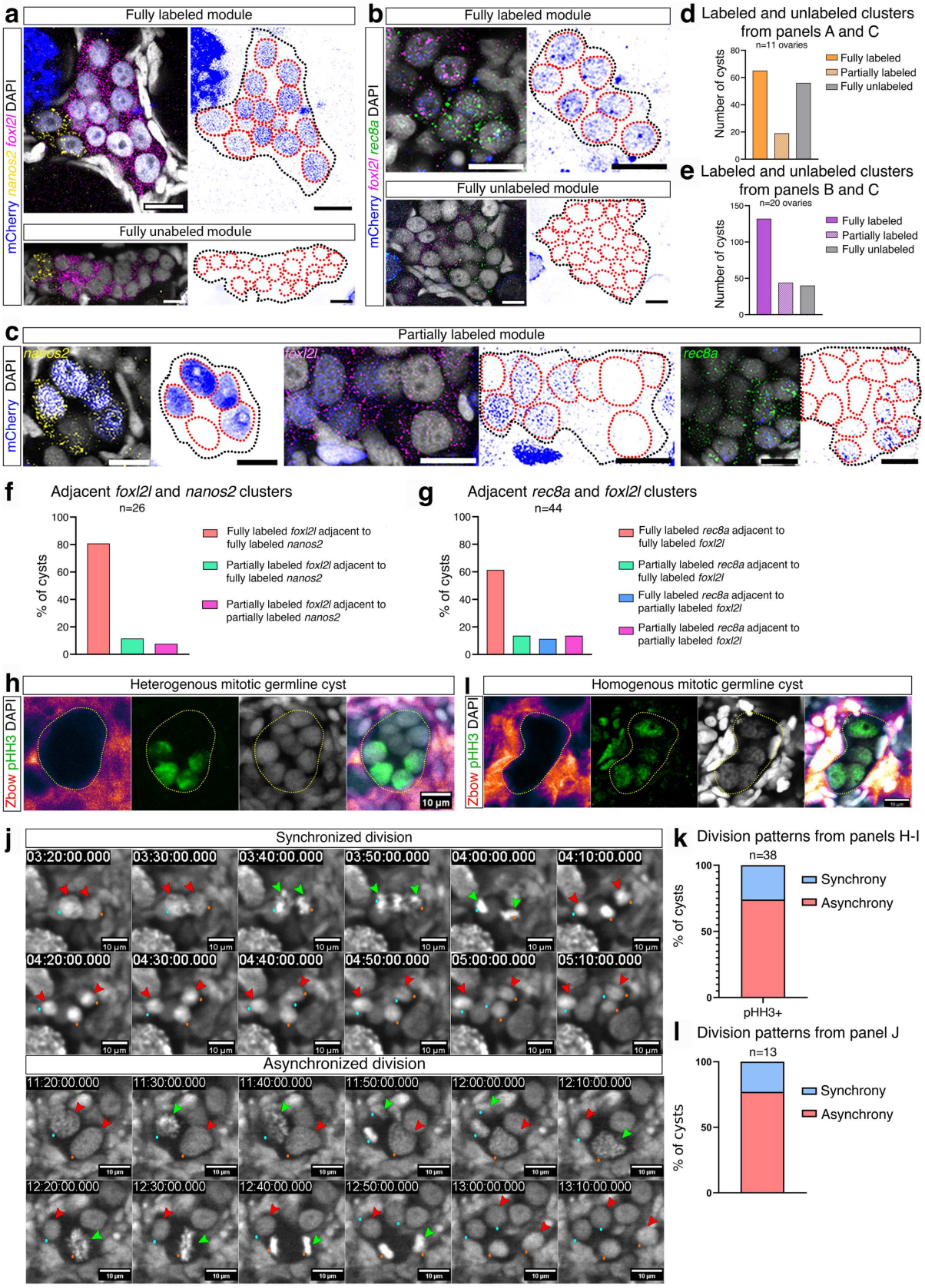

1248 **Figure 3. Dynamics of module development. a-e.** Lineage tracing of module cells from

early progenitors confirms spatially linear development in modules (Methods, see also Extended Data Fig. 3a-b). Ovaries were co-labeled for the lineage tracer (nuclear mCherry, blue) and multiplexed HCR-FISH for *nos2* (yellow), *foxl2l* (magenta), *rec8a* (green). Merged (left panels) and mCherry (right) channel images are shown. Modules are outlined in black and nuclei in modules are outlined in red. For each *nos2* + *foxl2l* and *foxl2l* + *rec8* pairs, fully mCherry-labeled traced clusters (all nuclei are mCherry+, a-b top) and fully mCherry-unlabeled traced clusters (all nuclei are mCherry(-), a-b bottom) were detected. See also Extended Data Fig. 3c. A third category - partially mCherry-labeled stage specific clusters are shown in c. Note some nuclei are mCherry+ and some are mChery(-) for each *nos2,* or *foxl2l*, or *rec8* stage specific clusters. The distribution of all categories of traced clusters from a-c is plotted in d-e. n=number of ovaries. See also Extended Data Fig. 3c. **f-g.** The distribution of *foxl2l*+ clusters that are adjacent *nos2*+ clusters (f) and of *rec8*+ clusters that are adjacent to *foxl2l*+ clusters (g) from all labeling categories in a, b, e, are plotted. n=number of clusters from 11 ovaries in f and from 20 ovaries in g. **h-l.** Oogonia divide non-synchronously. **h-i.** Ovaries co-labeled for somatic cells (fire LUT), pHH3 (green), and DAPI (grey) show heterogenous mitosis in oogonial cysts (outline). Either heterogenous (some nuclei are pHH3+ and some are pHH3(-), left) or homogenous cysts (all nuclei are pHH3+, right) were detected. The distribution of synchronized and asynchronized cysts is plotted in **k**. n=number of cysts from 10 ovaries. **j.** Live time-lapse imaging of *Tg(h2a:H2A-GFP)* (greyscale) ovaries detects both cases of synchronized (top) and asynchronized (bottom) divisions. Sum projection montages are shown with indicated timepoints. Non-dividing (red arrowheads) and dividing (green arrowheads) nuclei are indicated, and mother- and daughter-cells are labeled with color-coded dots. The distribution of synchronized and asynchronized cases is plotted in **l**. n=number of cysts from 3 ovaries. See additional examples in Extended Data Fig. 3D. Videos of all examples are shown in Supplementary Videos 6-9. Scale bars in all panels are 10 μm.

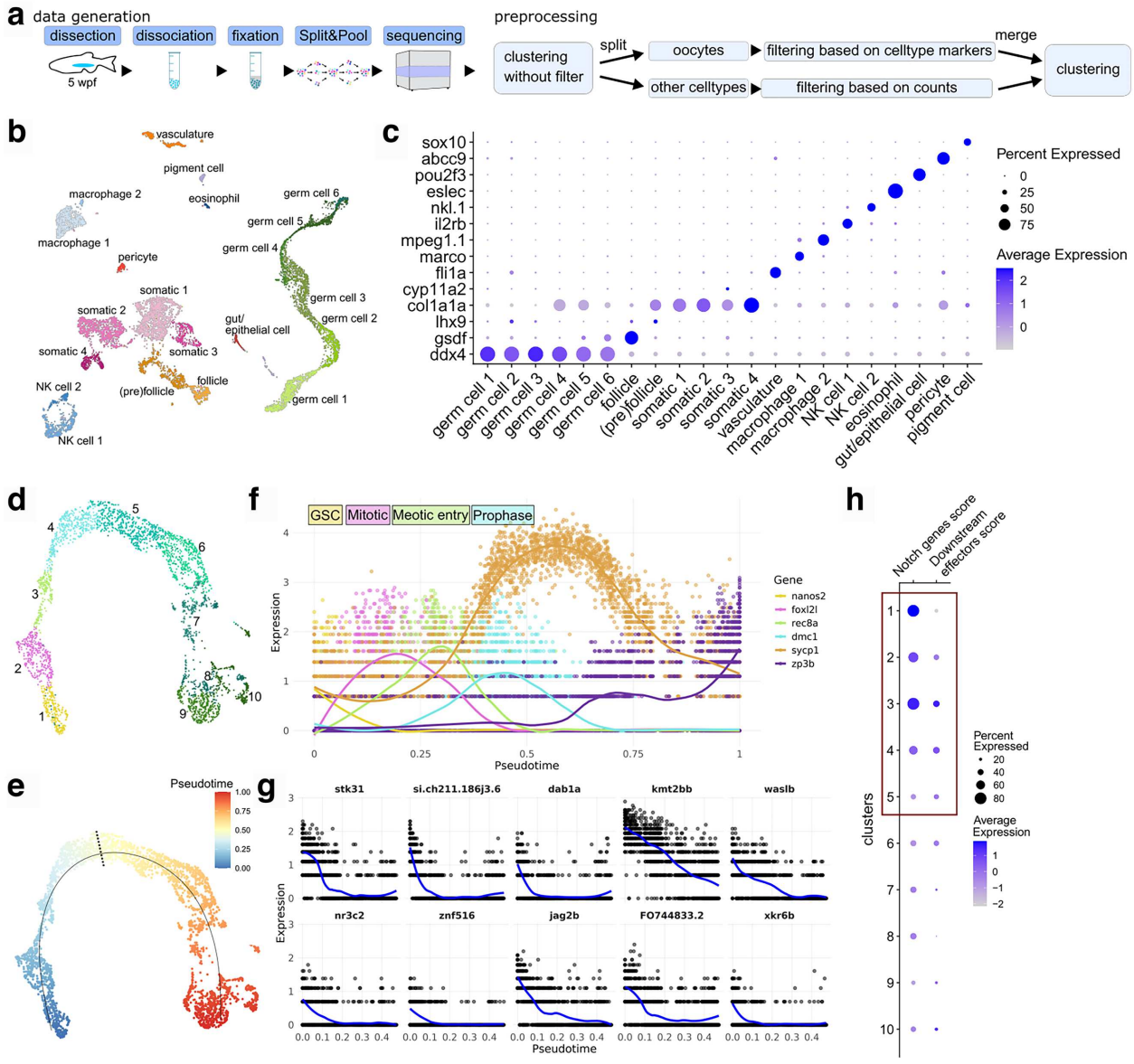

Figure 4. Profiling of ovarian cells and transcriptomic recapitulation of module architecture. a. Schematic of data generation and preprocessing pipeline (Methods, see also Extended Data Fig. 4-5). **b**. UMAP representation of scRNAseq dataset. **c**. Marker genes expressed in cell type clusters (see also Extended Data Table 2). **d**. Subclustering of germ cell clusters 1-6, first four clusters corresponding to *nos2*, *foxl2l*, *rec8a* and *dmc1* positive cells (see also Extended Data Table 3) **e**. Pseudotime of oocyte differentiation calculated with Scorpius. Dotted line indicates the pseudotime period (early oogenesis) used for calculation of gene correlations. **f**. Marker gene expression across full pseudotime trajectory. Expression values correspond to normalized expression in Pearson residuals. Points represent individual cells, and

lines show smoothed trends using LOESS regression. **g**. Top 10 genes correlated to *nos2* expression ranked by positive Spearman correlation coefficient. Significance was assessed using Spearman correlation with Benjamini–Hochberg correction for multiple testing (see also Extended Data Fig. 6 and Extended Data Table 4) **h**. Module scores for Notch genes and downstream effectors over oocytes clusters.

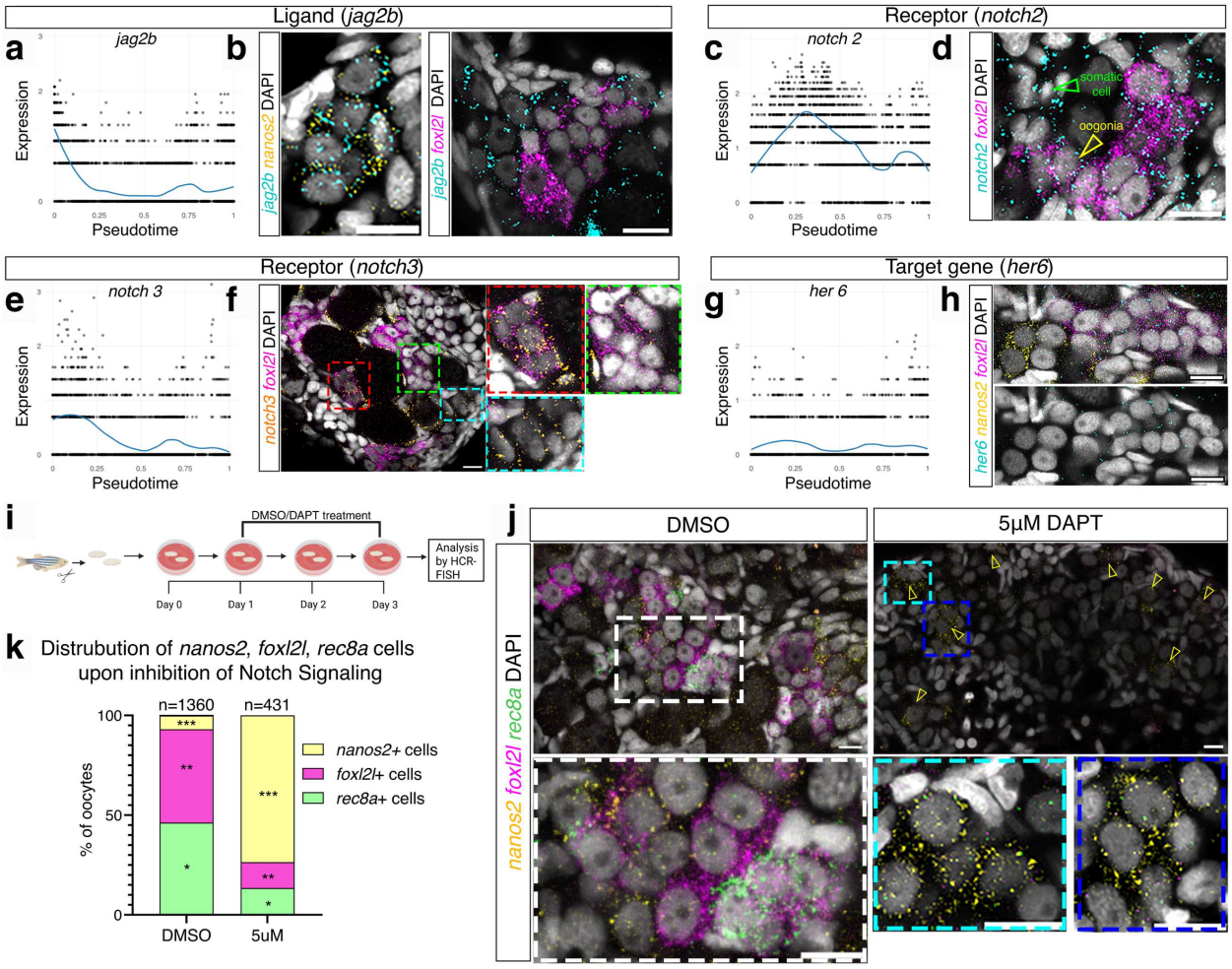

Figure 5. Notch signaling suppresses GSC fate and promotes oocyte differentiation within modules. a-h. Expression of Notch pathway components identified from scRNA-seq in relevant module cells. For each gene gene, expression form scRNA-seq and multiplexed HCR-FISH images for the corresponding gene and the oocyte developmental markers are shown. **a-b.** The Notch ligand *jag2b* (cyan) is expressed in *nos2*+ (yellow) cells, but not in adjacent *foxl2l*+ (magenta) cells. **c-d.** The Notch receptor *notch2* (cyan), is expressed in *foxl2l*+ (magenta) cells and in somatic cells, as indicated. **e-f.** The Notch receptor *notch3* (orange) is expressed in some but not all *foxl2l*+ (magenta) cells, as well as in *foxl2l(-)* cells. Right panels are zoom-in images of boxes in left panel. **g-h.** The Notch target gene *her6* (cyan) is expressed in *foxl2l*+ cells but not in *nos2*+ cells. n=3-7 ovaries per probe combination in a-h. Expression values over Pseudotime correspond to normalized expression in Pearson residuals. Points represent individual cells, and lines show smoothed trends using LOESS regression. **i.** Schematic experimental design for Notch signaling inhibition in *ex-vivo* ovary culture. **j.** DMSO and DAPT-treated ovaries form

experiments in i were co-labeled for multiplexed *nos2* (yellow), *foxl2l* (magenta), *rec8a* (green), and DAPI (grey). Entire modules are detected in control DMSO-treated ovaries. In contrast, DAPT-treated ovaries exhibit an increase in *nos2*+ cells (arrowheads) and lack of complete modules. Bottom panels are zoom-in images of boxes in top panels. The percentage of each *nos2*+, *foxl2l*+, and *rec8*+ cells in DMSO- versus DAPT-treated ovaries s plotted in **k**. n=number of cells from 7 DMSO-treated ovaries, and 8 DAPT-treated ovaries. Scale bars in all panels are 10 μm.

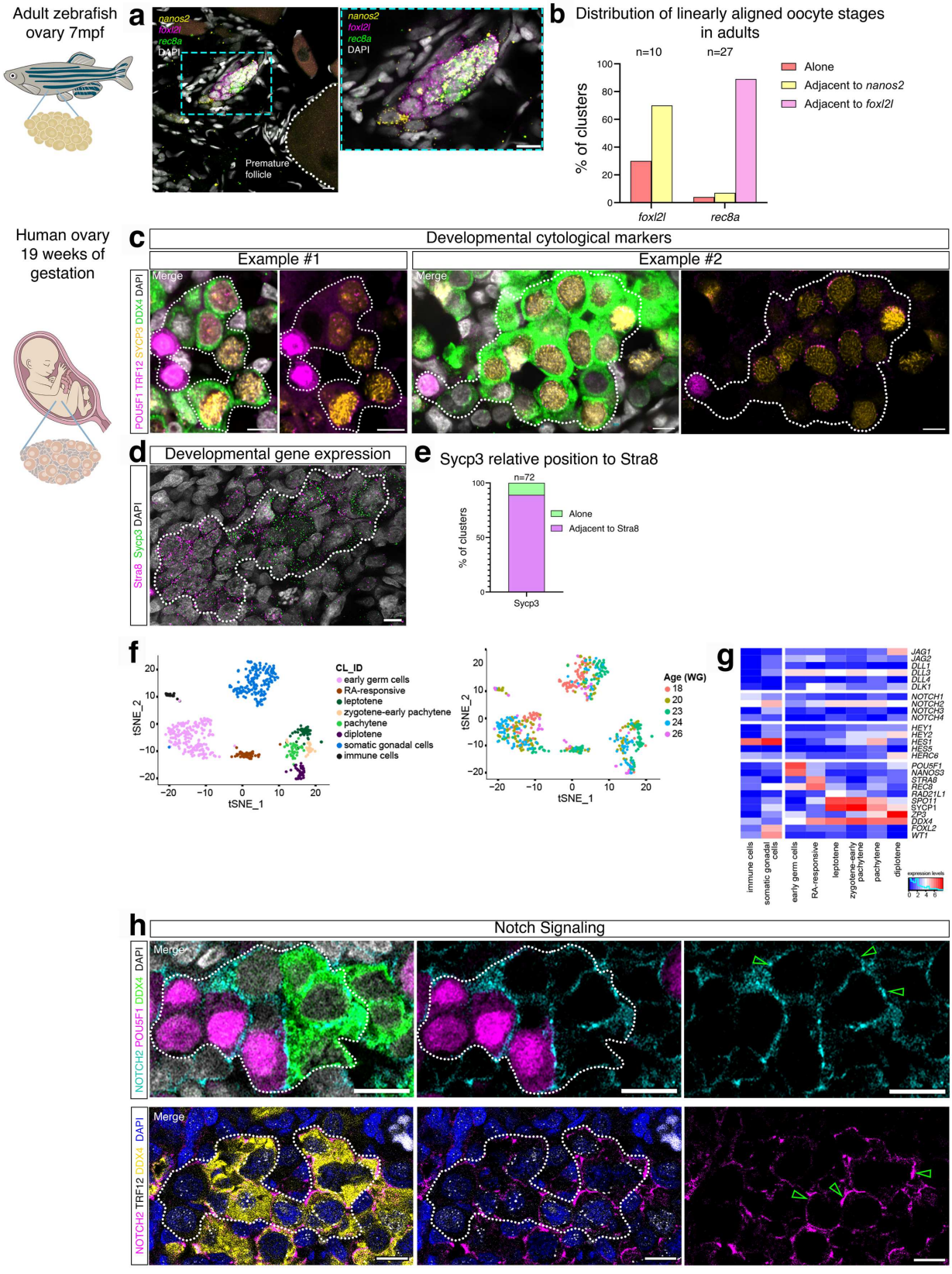

1350 **Figure 6. Adult zebrafish and prenatal human ovaries exhibit module-like**

organization. a-b. Adult 7 mpf ovaries co-labeled for multiplexed *nos2* (yellow), *foxl2l* (magenta), *rec8a* (green), and DPAI (grey), show developmental organization in ovarian modules similar to developing ovaries. The distribution of *foxl2l*+ clusters that are adjacent to *nos2*+ clusters and of *rec8*+ clusters that are adjacent to either *foxl2l*+ or *nos2*+ clusters is plotted in b. n=number of clusters from 6 ovaries. **c.** Ovarian modules are conserved in human fetal developing ovaries. Ovaries at 19 weeks of gestation (WG) co-labeled for POU5F1 (magenta), SYCP3 (yellow), TRF1/2 (magenta), DDX4 (green), and DAPI (grey), show POU5F1+ early germ cells at young tip of modules (white outlines), followed by meiotically progressing DDX4+SYCP+ cells, as detected by cytological meiosis markers. TRF1/2 shows telomere loading on the nuclear envelope at meiotic onset (leptotene) and clustering at zygotene, while on parallel SYCP3 shows progressive synaptonemal complex formation. Two examples of modules are shown. n=2 ovaries. **d-e.** Human ovaries as in C, co-labeled for multiplexed HCR-FISH for *STRA8* (magenta, meiosis induction) and *SYCP3* (green, meiotic prophase), and DAPI (grey), show developmental linear arrangement, with *SYCP3*+ cells located adjacent to *STRA8*+ cells. The distribution of *SYCP3*+ cells that are adjacent or not adjacent to *STRA8*+ cells is plotted in e. n=72 clusters from 2 ovaries. **f-g.** scRNAseq from human fetal ovaries 18-26WG colored by cluster identity (top) and weeks of gestation (bottom) in f. Heatmap showing the average expression of genes of interest per cluster in g. **h.** NOTCH2 receptor is expressed in human module cells. Human fetal ovaries as in c, were co-labeled for NOTCH2 (cyan) POU5F1 (magenta), DDX4 (green), and DAPI (grey) in top panels, and for NOTCH2 (magenta), TRF1/2 (white), DDX4 (yellow), and DAPI (blue) in bottom panels. NOTCH2 is mostly detected in Ddx4+ cells adjacent to POU5F1+ cells, and in early meiotic cells (TRF1/2 loaded on nuclear envelope; leptotene), suggesting expression in progenies of POU5F1+ cells and in meiotic prophase, as detected by scRNAseq in f-g, and similar to expression of Notch receptors in zebrafish modules. n=2 ovaries. Scale bars in all panels are 10 μm.

Extended Data Figures and Legends

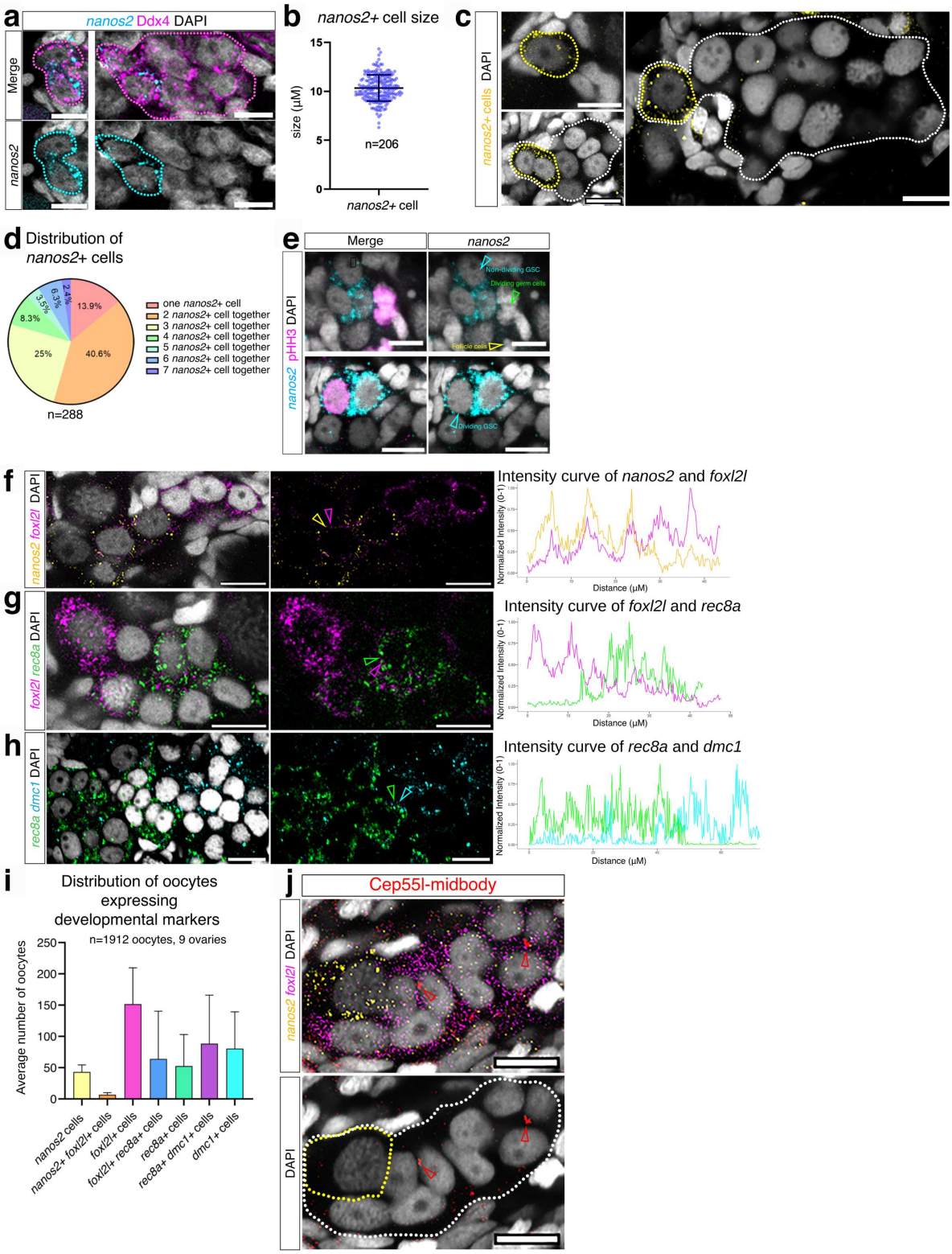

Extended Data Fig. 1 Supporting information for Figure 2. a. Co-labeling of *nos2* (cyan) by FISH and for Ddx4 (magenta) immune-fluorescence (IF) and DAPI (grey) confirms *nos2*+

germ cell identity. **b.** Measurements of *nos2* + cell size (diameter, measured as in[28]. Average size=10.35 μm, n=number of cells from 27 ovaries. **c.** Examples of the distribution of *nos2* (yellow, yellow outline) cells, showing a solitaire cell (top left), cells adjacent to oogonia (white outline, bottom left), and cells adjacent to oogonia and a full module (white outline, right). **d.** The distribution of *nos2*+ cell groups. n= number of cells from 27 ovaries. **e.** Some nos2+ cells are actively dividing and some are not. Co-labeling of *nos2* (cyan) FISH and pHH3 (magenta) IF, and DAPI (grey). Top: Dividing *nos2*(-) germ cells and non-dividing *nos2*+ GSC. Bottom: Dividing *nos2*+ GSC. Arrowheads point to cell types as indicated. **f to i.** Multiplex HCR of consecutive developmental marker genes in ovaries co-labeled with DAPI as in Figure 2h-j, and their corresponding normalized intensity plots show co-expression of markers (gene color-coded arrowheads) in likely transitioning cells. The distribution of all stage-specific and transitioning cells from our experiments in Fig. 2h-j and here is plotted in i. **j.** Cep55l (red, red arrowheads) ovaries multiplexed for *nos2* (yellow) with *foxl2l* (magenta) and DAPI (grey) as in Fig. 1l, show interconnecting CBs between *foxl2l*+ cells, but not between *nos2*+ cells or between *nos2*+ and foxl2l+ cells. Scale bars in all panels are 10 μm.

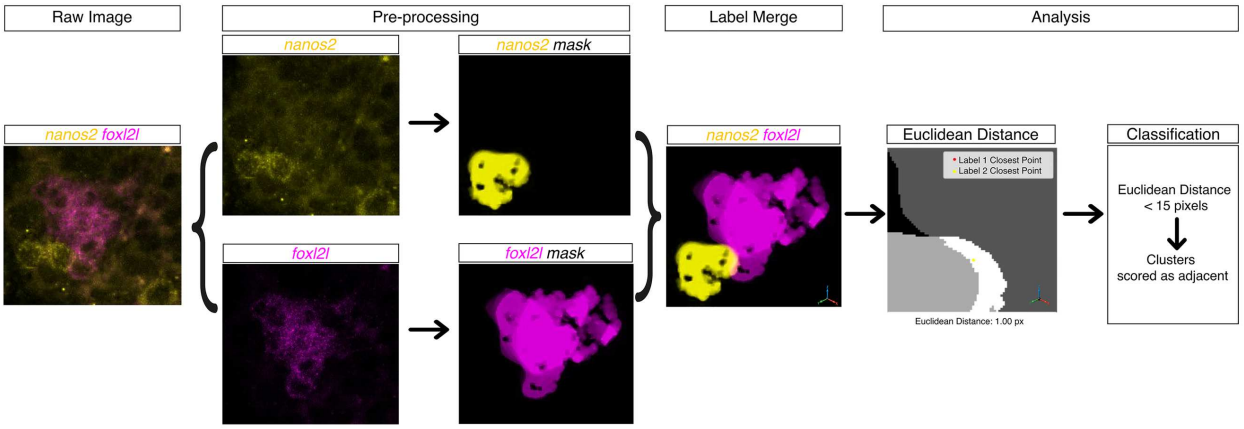

Extended Data Fig. 2. Schematic outline of 3D Euclidean distance-based neighborhood analysis (Methods). Raw ROI image of multiplexed HCR-FISH from whole ovaries [*nos2* (yellow) and *foxl2l* (magenta) are shown as an example] undergo the following steps as indicated (detailed in Methods). Pre-processing of input signal creates segmented label mask for each marker gene. Labels are then merged for analysis while preserving original 3D information, and the 3D Euclidean distance is computed between the label pairs for neighborhood analysis. Pairs are classified as "adjacent" if the distance is $\leq$ 15, and "not adjacent" is the distance is >15.

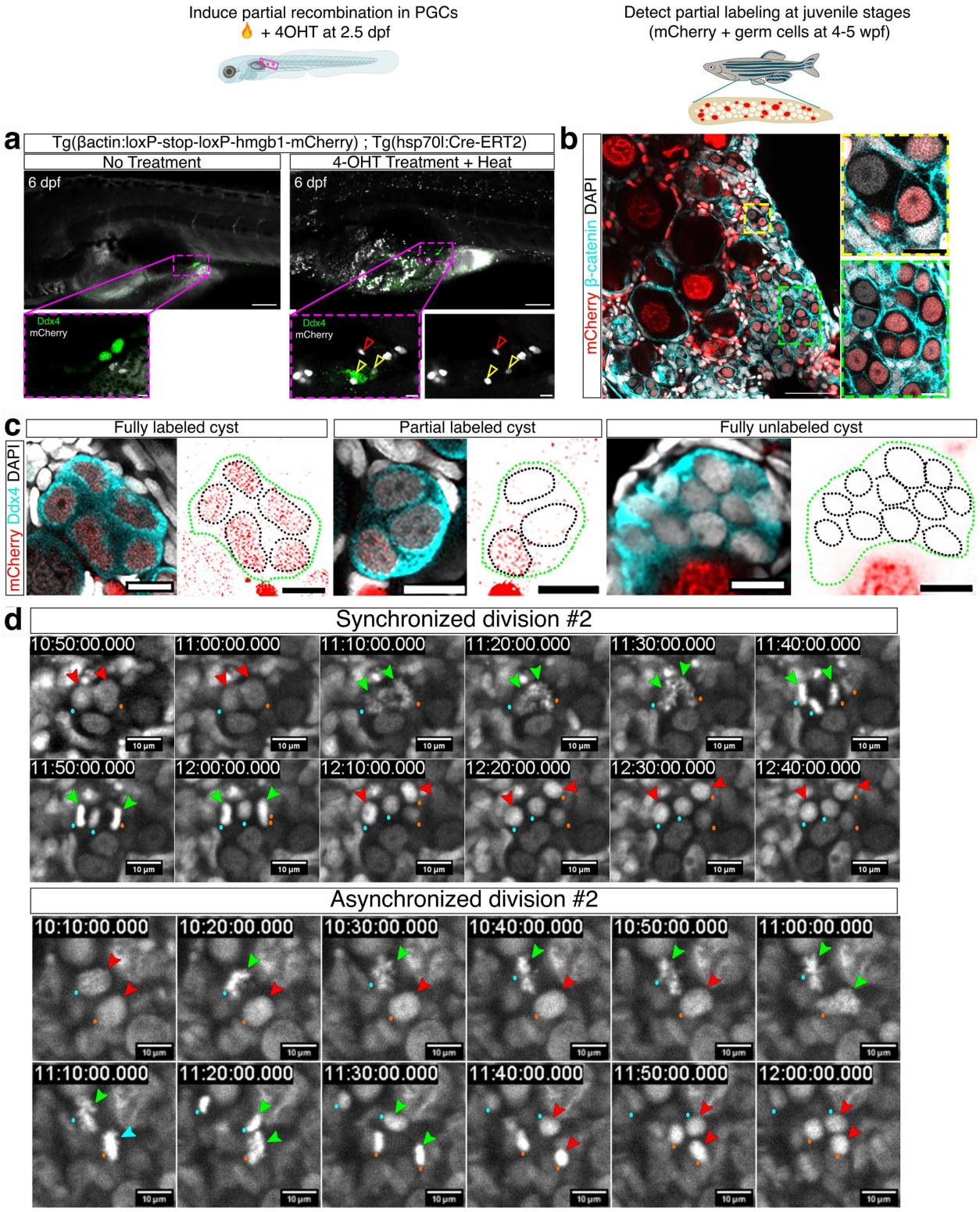

Extended Data Fig. 3. Supporting information for Figure 3. a-b. Lineage tracing experimental design. Cre recombination of floxed mCherry is induced by heat-shock and 4-OHT treatments at 2.5 dpc (a), resulting in partial recombination as detected at 6 dpf, by nuclear

mCherry signals (greyscale) in Ddx4+ PGCs (green, yellow arrowheads), and Ddx4(-) somatic cells (red arrowheads). Top: larval view of future gonad region (magenta boxes). Bottom: zoom-in images of the magenta boxes. Treated larvae are raised to juvenile stages where partial recombination is detected in 5 wpf ovaries (b). Ovaries were co-labeled for mCherry (red), β-catenin (cyan, and DAPI (grey), showing partial recombination throughout the ovary. Left: ovary overview, right: zoom-in images of the color-coded boxes in left panel. **c.** Co-labeling for Ddx4 (cyan), the lineage-tracer nuclear mCherry (red, black dashed outlines), and DAPI (grey), confirms the fully-labeled, partially labeled, and fully unlabeled clusters (green outlines) detected in Fig. 3a-c. Scale bars in all panels are 10 μm. **d.** Live time-lapse imaging of *Tg(h2a:H2A-GFP)* (greyscale) ovaries in Fig. 3j, showing additional examples of synchronized (top) and asynchronized (bottom) divisions. Videos of all examples are shown in Supplementary Videos 6-9.

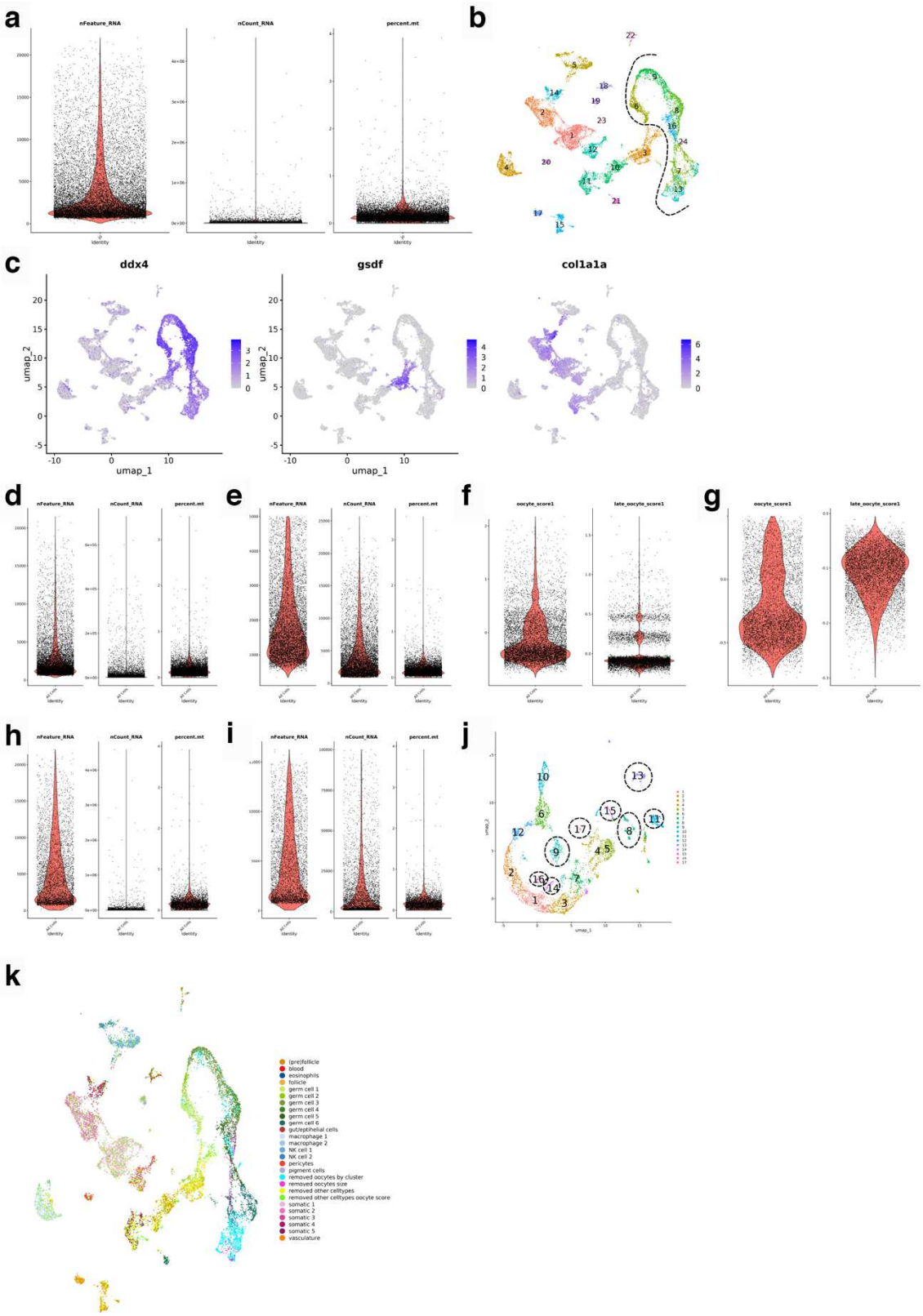

Extended Data Fig. 4. Supporting information of preprocessing pipeline on main

dataset shown in Figure 4. **a.** Quality metrics for all cells before filtering. nFeature_RNA corresponds to genes per cell, nCounts_RNA corresponds to transcripts per cell and percent.mt is the calculation for mitochondrial reads per cell. The mitochondrial percentage is low compared to commercial microfluidics techniques, possibly due to fixation early in the protocol. **b.** UMAP representation of all cells. The dotted line indicates separation of cells into oocytes (right) and other celltypes (left). **c.** Gene expression of ddx4, gsdf and col1a1a plotted on all cells to identify two subsets for splitting. **d.** Quality metrics for "other cell types" before filtering for gene and transcript counts. **e.** Quality metrics for "other cell types" after filtering for gene and transcript counts. **f.** Quality metrics for "other cell types" before filtering for oocyte and late_oocyte score. **g.** Quality metrics for "other celltypes" after filtering for oocyte and late_oocyte score. **h.** Quality metrics for "oocytes" before filtering for transcript counts. **i.** Quality metrics for "oocytes" after filtering for transcript counts. **j.** UMAP representation of oocytes. Dotted circles indicating removed clusters because of marker gene expression of other cell types. **k.** UMAP representation of all cells before filtering, colored by assigned cell type or in which step they were removed.

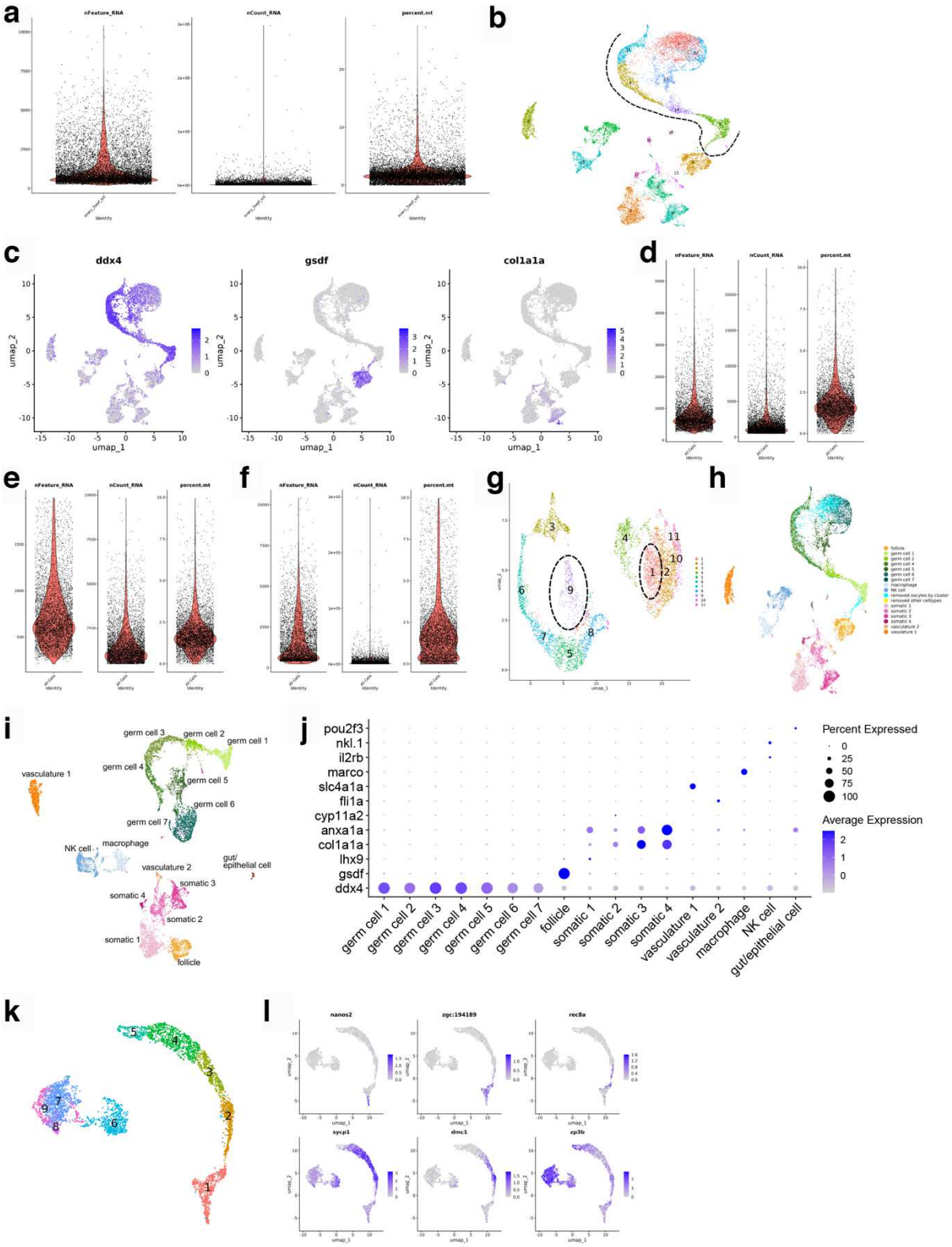

Extended Data Fig. 5. Supporting information for additional 10X dataset, preprocessing pipeline and cell type clustering. a. Quality metrics for all cells before filtering. nFeature_RNA corresponds to genes per cell, nCounts_RNA corresponds to transcripts per cell

and percent.mt is the calculation for mitochondrial reads per cell. Cells were filtered for <10% mitochondrial reads. **b**. UMAP representation of all cells. The dotted line indicates separation of cells into oocytes (right) and other celltypes (left). **c.** Gene expression of *ddx4*, *gsdf* and *col1a1a* plotted on all cells to identify two subsets for splitting. **d**. Quality metrics for "other cell types" before filtering for gene and transcript counts. **e**. Quality metrics for "other cell types" after filtering for gene and transcript counts. Cutoffs set to 2000 for nFeature_RNA and 10000 for nCount_RNA. **f**. Quality metrics for "oocytes" before filtering for clusters. **g**. UMAP representation of oocytes. Dotted circles indicate clusters that were removed because they express marker genes of other cell types. **h**. UMAP representation of all cells before filtering, colored by assigned cell type or step in which they were removed. **i**. UMAP representation of cell types after preprocessing. **j**. Marker genes expressed in cell type clusters: Less resolution in immune cells compared to Split&Pool approach. No pre-follicle, pericytes, pigment cells detected. **k**. Sub-clustering of germ cell clusters 1-7. **l**. Feature plot of marker genes for early oogenesis, later stages of oocytes with more representation than early stages. Not enough resolution in transcriptomic data to cluster marker genes in different clusters. *zp3b* expression shows ambient RNA contamination in earlier clusters.

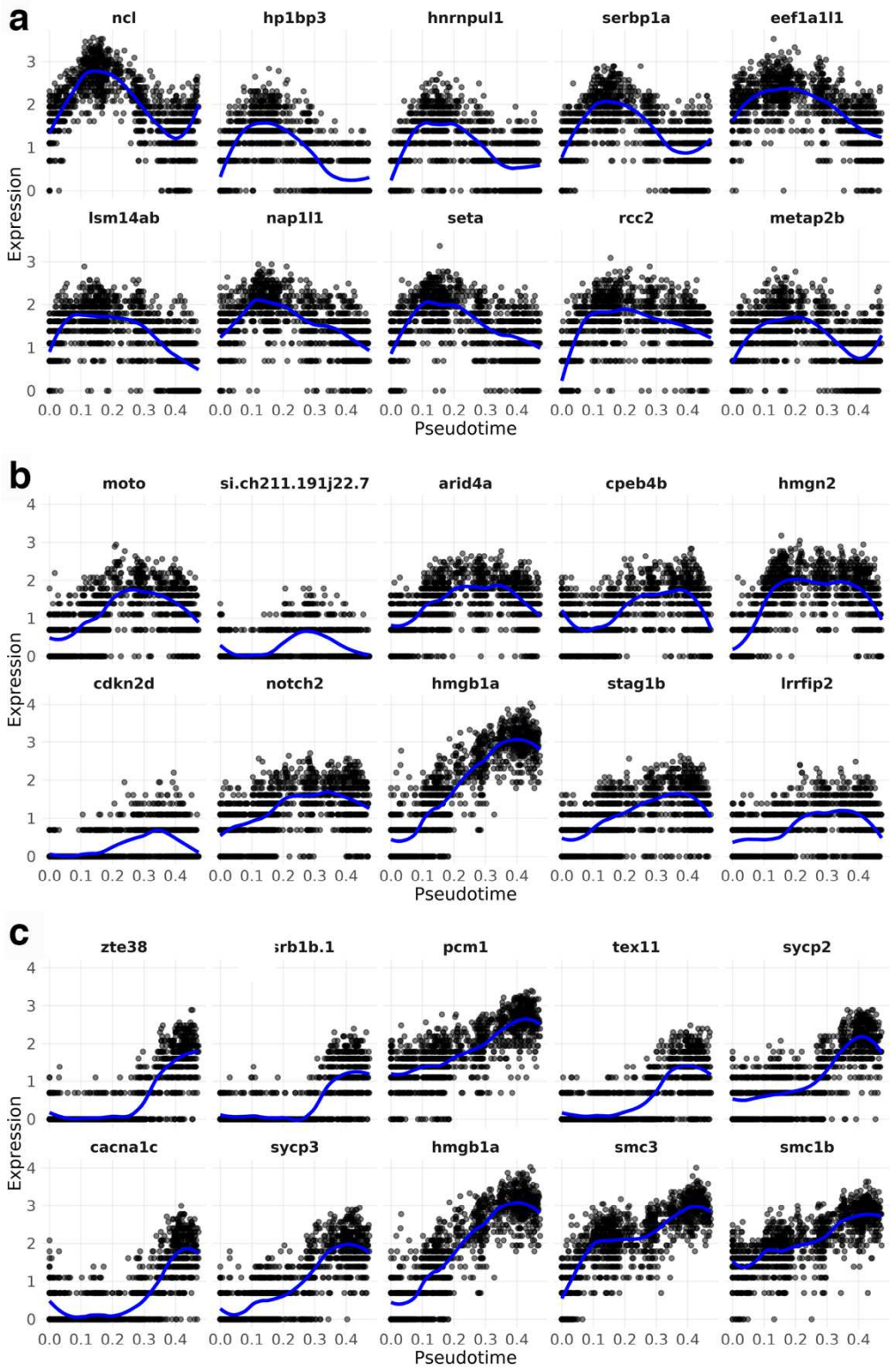

Extended Data Fig. 6. Supporting information for Figure 4G. a. Top 10 genes correlated to *foxl2l* expression ranked by positive Spearman correlation coefficient. Significance was assessed using Spearman correlation with Benjamini–Hochberg correction for multiple

testing. **b**. Top 10 genes correlated to *rec8a* expression ranked by positive Spearman correlation coefficient. Significance was assessed using Spearman correlation with Benjamini–Hochberg correction for multiple testing. **c**. Top 10 genes correlated to *dmc1* expression ranked by positive Spearman correlation coefficient. Significance was assessed using Spearman correlation with Benjamini–Hochberg correction for multiple testing.

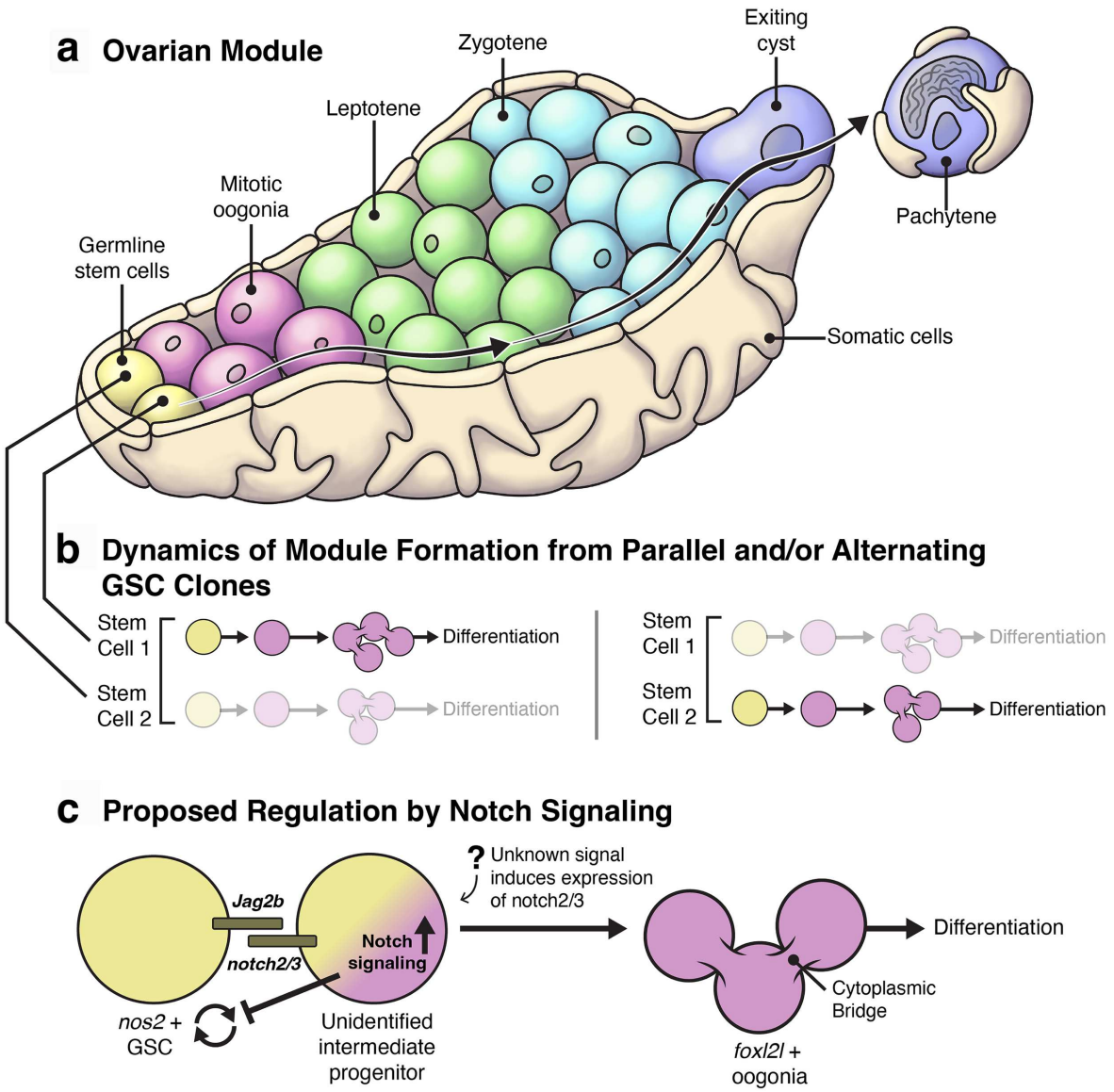

Extended Data Figure 7. Proposed model of oocyte production form GSCs in ovarian modules. a. In the morphogenetic unit of the modules, germ cells (color-coded for cell types and developmental stages) are collectively surrounded by somatic cells and develop spatially linearly. GSCs at the young tip produce oogonia (directly or via yet unknown intermediate progenitor, which is not depicted for simplicity). Oogonia undergo mitotic divisions and form germline cysts (interconnected CBs are not depicted for simplicity), and these cysts continue to progress linearly through meiosis (leptotene, zygotene), before forming the primordial follicle by the pachytene stage. **b.** Proposed lineage dynamics of development in modules. ≥2 lineages of GSC-to-developing oocyte clones are found in modules. We propose that individual GSC clones produce oogonia in parallel and/or in an alternating fashion, which in turn form cysts

and continue in meiosis. For simplicity only 2 clones are depicted. A non-active clone is indicated by higher opacity of the lineage diagram. The precise dynamics of parallel and/or alternating clones, and whether they are random or controlled, remains to be determined. **c.** Proposed mechanism for Notch regulation of GSCs. Nos2+ GSCs express the Notch ligand Jag2b. We hypothesize that at some point expression of Notch2/3 receptors is initiated (either stochastically and/or by a yet unknown signal) in a subset of these cells, which may represent an intermediate progenitor. The newly receptor-expressing cell/s become competent to receive the Jag2b signal from adjacent *nos2*+ cells and respond by activating the Notch signaling pathway. Notch activity in these cells suppresses the *nos2* fate and promotes a *foxl2l* fate, generating oogonia which in turn proceed in forming cysts and progressing through differentiation.

Supplementary Videos legends

Supplementary Video 1. Supporting information for Fig. 1e. 3D view of the module shown in Fig. 1e. The video shows the stack sections followed by 3D reconstruction and 3D view of somatic cells (orange arrows, labeled by the transgenic *zebrabow* line), showing no invasion of somatic cells between oocytes at different stages. Scale bar is 5 μm.

Supplementary Video 2. Supporting information for Fig. 1h. 3D view of the module shown in Fig. 1h. 3D view is followed by segmentation of *foxl2l*+ cells (magenta) and of somatic cells (cyan, labeled by the transgenic *zebrabow* line), showing opening of somatic cell protrusions between *foxl2l*+ and *foxl2l*- cells. Scale bar is 10 μm.

Supplementary Video 3. Supporting information for Fig. 1k. 3D segmentation of the SBF-SEM data from Fig. 1k, showing leptotene and zygotene clusters inside a module. Scale bar is 50 μm.

Supplementary Video 4-5. Supporting information for Fig. 1l. 3D segmentation of the cells shown in Fig 1l, showing interconnected (CB, Cep55l, red) *foxl2l*+ (magenta) and *rec8a*+ (green) cells in Supplementary Video 4, and interconnected *rec8a*+ (green) and *dmc1*+ (cyan) cells in Supplementary Video 5. Scale bar is 5 μm.

Supplementary Video 6-7. Supporting information for Fig. 3j. Live time-lapse images of synchronous cell division from Fig. 3j and Extended Data Fig. 3D. Scale bar is 10 μm.

Supplementary Video 8-9. Supporting information for Fig. 3j. Live time-lapse images of asynchronous cell division from Fig. 3j and Extended Data Fig. 3D. Scale bar is 10 μm.

Supplementary Data file captures

Extended Data Table 1. scRNAseq Library specification and sequencing quality metrics.

Extended Data Table 2. Top 50 enriched marker genes for all celltype clusters in Fig 4B.

Extended Data Table 3. Top 50 enriched marker genes for all oocyte clusters in Fig 4D.

Extended Data Table 4. Gene correlation scores and p values for top 100 genes correlated to the marker genes of early oogenesis (nanos2, foxl2l, rec8a and dmc1).

Supplementary Files

This is a list of supplementary files associated with this preprint. Click to download.

- SupplementaryVideo8.avi
- SupplementaryVideo2.mp4
- SupplementaryVideo7.avi
- SupplementaryVideo6.avi
- SupplementaryVideo9.avi
- SupplementaryVideo4.mp4
- SupplementaryVideo5.mp4
- SupplementaryVideo3.mp4
- SupplementaryVideo1.mp4